(NASA-CR-165203) SPHERICAL ROLLER BEARING ANALYSIS. SKF COMPUTER PROGRAM SPHERBEAN. VOLUME 1: ANALYSIS Final Report, Jun. 1978 - Dec. 1980 (SKF Technology Services) 86 p HC A05/MF A01 CSCL 13I G3/37

N82-20540

Unclas 09303

SPHERICAL ROLLER BEARING ANALYSIS

SKF COMPUTER PROGRAM "SPHERBEAN"

VOLUME I: ANALYSIS

DECEMBER 1980

R. J. Kleckner

J. Pirvics

SKF REPORT NO. AT81D006 SKF PROGRAM NO. AT81Y001

SUBMITTED TO:

NATIONAL AERONAUTICS & SPACE ADMINISTRATION
LEWIS RESEARCH CENTER
21000 BROOKPARK ROAD
CLEVELAND, OHIO 44135

UNDER CONTRACT NAS3-20824

SUBMITTED BY:

SKF TECHNOLOGY SERVICES
SKF INDUSTRIES, INC.
KING OF PRUSSIA, PA

1. Report No.	2. Government Accession No.	3. Recipient's Catalog No.
CR-165203		

4. Title and Subtitle
SKF Computer Program SPHERBEAN
Volume I: Analytic Formulation

5. Report Date
December 1980

6. Performing Organization Code

7. Author(s)
Robert J. Kleckner and
Juris Pirvics

8. Performing Organization Report No.
AT81D006

9. Performing Organization Name and Address
SKF Industries, Inc.
Technology Services
1100 First Avenue
King of Prussia, Pa. 19406

10. Work Unit No.

11. Contract or Grant No.
NAS3-20824

12. Sponsoring Agency Name and Address
NASA/Lewis Research Center
21000 Brookpark Road
Cleveland, Ohio 44135

13. Type of Report and Period Covered
Final Report/June 1978-December 1980

14. Sponsoring Agency Code

15. Supplementary Notes

16. Abstract

The objective of this three volume report is to describe the use of a fully operational computer program which will predict the thermomechanical performance characteristics of high speed lubricated double row spherical roller bearings. The analysis allows six degrees of freedom for each roller and three for each half of an optionally split cage. Roller skew, free lubricant, inertial loads, appropriate elastic and friction forces, flexible outer ring, etc. are considered. Roller quasidynamic equilibrium is calculated for a bearing with up to 30 rollers per row, and distinct roller and flange geometries are specifiable. Software performance is verified by correlation with results of hardware testing.

Volume II is structured to guide the user in the correct and practical implementation of SPHERBEAN. Input and output, guidelines for program use and sample executions are detailed.

Volume III describes the results of a series of full scale hardware tests, and demonstrates the degree of correlation between performance predicted by SPHERBEAN and measured data.

The material presented in this, Volume I, describes the models and associated mathematics used within SPHERBEAN. The user is referred to the material contained here for formulation assumptions and algorithm detail.

17. Key Words (Suggested by Author(s))
Spherical Roller Bearing
Computer Simulation
Spherical Planet Bearing
Roller Skew
High Speed
Thermal Analysis

18. Distribution Statement

19. Security Classif. (of this report)	20. Security Classif. (of this page)	21. No. of Pages	22. Price*

* For sale by the National Technical Information Service, Springfield, Virginia 22161

NASA-C-168 (Rev. 10-75)

SPHERICAL ROLLER BEARING ANALYSIS

SKF COMPUTER PROGRAM "SPHERBEAN"

VOLUME I: ANALYSIS

DECEMBER 1980

R. J. Kleckner
J. Pirvics

Prepared:

Approved:

Released:

SKF REPORT NO: AT81D006

SKF PROGRAM NO: AL81Y001

SUBMITTED TO:

NATIONAL AERONAUTICS AND SPACE ADMINISTRATION
LEWIS RESEARCH CENTER
21000 BROOKPARK ROAD
CLEVELAND, OHIO 44135
UNDER CONTRACT NAS3-20824

SUBMITTED BY:

SKF INDUSTRIES, INC.
TECHNOLOGY SERVICES
1100 FIRST AVENUE
KING OF PRUSSIA, PA 19406

FOREWORD

This, Volume I of the report "Spherical Roller Bearing Analysis" documents the analysis, program design and algorithm detail employed in the generation of the computerized analytic design tool SPHERBEAN. Efforts involved in the generation of the code were accomplished under contract NAS3-20824 issued by the NASA-Lewis Research Center of Cleveland, Ohio and administered by the Structures and Mechanical Technologies Division. Funding was provided by the Product Assurance office of the Army Aviation Research and Development Command, St. Louis, Missouri. The technical monitor was Mr. H. H. Coe. The work was performed at SKF Industries, Inc., King of Prussia, Pennsylvania, during the period June 1978 to December 1980.

Technical project leadership was executed by Mr. R. J. Kleckner, with contributions from Dr. J. Pirvics and Messrs. G. Dyba and T. Deromedi.

TABLE OF CONTENTS

PAGE

F-4185C-1-R100

LIST OF FIGURES

LIST OF TABLES

F-4185C-1-R100

NOMENCLATURE

C_g	Cage rail/ring land radial clearance (M)
C_D	Drag coefficient for fluid flow over a cylinder
E'	$\left(\frac{1-\nu_1^2}{\pi E_1} + \frac{1-\nu_1^2}{\pi E_2} \right)^{-1}$, (N/M^2)
E_1, E_2	Elastic moduli for bodies 1 and 2 (N/M^2)
f_A	Lubricant parameter given in [19]
G	Lubricant coefficient of thermal expansion $(1/C^o)$
h_0	Film thickness (M)
$\hat{i},\hat{j},\hat{k}$	Unit vectors along the x,y,z axis, respectively
K_L	Lubricant parameter given in [18]
M	Roller mass (kg)
n	Number of rollers per row
n_g	Number of cage guide rails
n_r	Number of rows of rollers
n_s	Number of slices
n_t	Total number of rollers
$\dot{q}$	Heat generation rate (watts)
r_g	Equivalent cage rail radius (M), see equation (25)
$\underline{V},\underline{U}$	Sliding and entrainment velocity vectors (M/sec)
w_g	Equivalent width of cage guide rail (M), see equation (26)
α	Pressure-viscosity coefficient at elevated temperature (M^2/N)

NOMENCLATURE (continued)

ε	Eccentricity
η_0	Lubricant viscosity at ambient pressure, and elevated temperature (N-sec/M^2)
ν	Kinematic viscosity (CS)
ν_1, ν_2	Poisson's ratios for bodies 1 and 2
ρ	Lubricant density at elevated temperature (gm/cm)
ρ'	Curvature sum, $\frac{1}{r_1} + \frac{1}{r_2}$ (1/M)
ρ_{16}	Lubricant density at 16^{o}C (60^{o}F), (gm/cm^3)
σ	Contact stress (N/M^2)
τ	Lubricant shear stress (N/M^2)
τ_C	Critical shear stress, 6.89 x 10^6 N/M^2 (1000 psi)
ϕ_S	High contact stress factor

SUBSCRIPTS/SUPERSCRIPTS

i	Refers to the i-th roller, i = 1,2,......., n_t
j	Refers to the j-th row of rollers
k	Refers to the k-th slice, k = 1,2,...., 20
m	Refers to the m-th raceway, m = 1, outer, m = 2, inner.

NOTATION

$\underline{a}$	A vector with components a_x, a_y, a_z
$\lvert\underline{a}\rvert$	Magnitude of vector $\underline{a}$
$(\vec{x})$	Vector cross product, $\underline{a} \vec{x} \underline{b} = \underline{c}$
$(\bullet)$	Vector dot product, $\underline{a} \bullet \underline{b} = d$

F-4185C-1-R100

1.0 INTRODUCTION

The general class of load support systems (LSS) consists of mechanical assemblies which transfer force and moment vectors. The transfer is constrained to maintain component displacements within prescribed, and frequently severe limits.

Shaft mounted rolling element bearings form a subset of the general LSS class. They are characterized by high load carrying capacity, low power loss, relative insensitivity to load fluctuation, rotation reversal and tolerance for start stop operation and reversal of rotation direction.

Various rolling element bearing configurations have evolved to service specific application requirements within this subset. The angular contact ball bearing, for example, supports combined loading and tolerates some misalignment. Because rolling elements with "line" as compared to "point" contact conjunctions offer superior capacity for a given design volume, bearings having tapered and cylindrical roller geometries have evolved to support large loads.

The relative displacement of components is a physical reality wherever mechanical assemblies transfer force. Structural elements distort within the generally asymmetric assembly and cause the misalignment of bearing raceways. This departure from the idealized "rigid" assembly can be controlled but not eliminated by manufacture, assembly and operation. In the presence of such deflections, and the associated misalignment, line contact geometries can be optimized only for a specific single load condition [1][1]. Severe penalties, in bearing life and operating performance, are sustained during less than optimum load support.

The self aligning spherical rolling element bearing, Figure 1, answers some shortcomings of the bearing types noted above. The geometry is unique. At low loads, the load vector is transferred by point contacts. At higher loads, modified line contacts perform this function. The bearing also supports combined radial and axial loading. This versatility has led to successful implementation in the large load support systems required by steel, paper and marine industries. Smaller mechanical assemblies, such as planetary gear reduction sets, have also seen successful application.

The rolling element bearing subset of the LSS class, in today's technology, is being required to operate at ever increasing DN values. Ball bearings, for example, have seen numerous high-speed applications up to the 2 X 10^6 DN level. Cylindrical and tapered roller configurations are being asked to follow in this regime. These new demands result from the requirements posed by advanced hardware missions and the increased emphasis on extracting maximum energy from a given process cycle. Basic

[1] Numbers in brackets denote references at end of report.

thermodynamics, particularly in mobile power plant design, dictates higher temperatures, stresses and speeds. Simultaneously, the assembly is required to occupy a decreased volume and weigh less. The combination of these parameters defines a lighter assembly, under increased stress, in a high temperature environment. Bearings, residing in assemblies of decreased structural rigidity, must sustain high, combined loads under conditions of misalignment and furthermore, do so at higher speeds.

The conventional spherical rolling element bearing design meets all but one of the challenges posed by these emerging requirements. Operating speed has been restricted to maximum values on the order of 5000 rpm. DN values have peaked at about $.25 \times 10^6$. Efforts are now under way to reach higher speeds. Particular emphasis is placed on reaching a 1.0×10^6 DN value.

The need to extend the operating DN regime for spherical roller bearings in new as well as current applications requires a realistic assessment of current methods for their design. Examination reveals that design relies on "rules", hand calculations, and some modest computerized simulations. The presence of mandated safety factors in rules for successful application reveals the measure of design performance buffers. At the same time, it reveals an opportunity for increasing performance and thus DN values to satisfy emerging load support needs.

Practical use of design reserves requires a more detailed understanding of, and the ability to predict, bearing performance within a load support system. The complexity of the interactions between the LSS and its environment requires an analytic/design tool to accurately describe the thermomechanical dialogue present [2]. Such a simulation tool can be created in the form of high speed digital computer software.

Several investigators have addressed the analysis of spherical rolling element bearings thus setting the stage for the required computerized simulation. Recently, Kellstrom [3] explored the fundamental mechanics which control symmetric roller behavior. He specifically addressed roller "self guidance" and explored the optimization of their skewing angles to minimize heat generation. Wieland and Poesl [4] have presented an interpretation of the empirical state of the art in spherical roller bearing design and application. Harris and Broschard [5] as well as Liu and Chiu [6] have examined these bearings in planetary gear applications in earlier investigations. Palmgren [7] and Harris [8] touch on computational procedures. Manufacturer catalog data and popularized applications articles serve to further highlight the need for a thorough analytic examination of the coupled phenomena which occur during spherical roller bearing operation.

This report documents the mathematical foundation for the analytic/design tool SPHERBEAN (SPHERical BEaring ANalysis). Specific algorithms, deviating from those of its cylindrical bearing sibling CYBEAN [9] and parent SHABERTH (SHAft BEaRing THermal analysis) [10], are described. Program architecture and solution methodology are likewise described which lead to SPHERBEAN'S capability to address quasidynamic equilibrium with consideration of EHD and HD forces at the raceway and flange, cage skew control, heat generation and centrifugal loads for single or double row designs having up to 30 rollers per row.

In Volume II [11] of this report, examples of program use are displayed with a description of computer resource needs. In Volume III [12] spherical bearing performance predicted by SPHERBEAN is compared to data obtained from full scale hardware tests.

2.0 COMPUTATION OF BEARING PERFORMANCE AT CONSTANT TEMPERATURE

Assume that a spherical roller bearing is to be simulated and that its performance is to be predicted as a function of physical dimensions, material properties and operating conditions. Then, the problem addressed is that of generating a computerized tool, specifically a tool which takes the form of a mathematical analog to a generalized physical configuration.

Consider a lubricated spherical roller bearing with its outer ring rigidly mounted in a supporting structure[2]. The inner ring accommodates a three dimensional load vector $\underline{P}$ imposed upon it by a shaft spinning at constant speed $\underline{\omega}$. Lubricant is applied at a known rate and occupies a fraction, ζ, of the free space in the bearing cavity. At a given instant in time, the bearing components and lubricant achieve the temperatures $T_c(^oC)$, c = 1,2,....,8. Here the subscript c refers to a specific component:

c = 1, outer ring	c = 5, flange, row 2
c = 2, inner ring	c = 6, bulk lubricant
c = 3, rollers	c = 7, shaft
c = 4, flange, row 1	c = 8, housing

The set of 13 quantities $\underline{P}$, $\underline{\omega}$, ζ, and T_c serve to define

[2]The planetary gear application is addressed in Section 2.4.

F-418SC-1-R100

the operating condition of the bearing.
Their values are considered known and sufficient to completely describe the bearing application.

Bearing response to a particular set of operating conditions is defined in terms of relative displacements and speeds.

An arbitrarily chosen reference state, from which component displacements are measured under applied loading, is shown in Figure 2. It is assumed that the outer ring, and therefore the outer ring reference frame, is fixed in space. The cage, inner ring and outer ring coordinate frames are coincident in this reference position, and the rollers are equally spaced and radially positioned so that at the point of closest approach to either raceway, a clearance equal to 1/4 the diametral clearance exists. Individual rollers are identified by their corresponding azimuthal position, Φ.

Inner ring response, shown in Figure 3, consists of pure translation, and is defined by the vector $\underline{a}$. The consideration of ring rotation has been omitted because of the self aligning capability of the bearing.

Roller displacement response is described by translation in a plane along the vector $\underline{b}$, and rotations about two axis defined by the quantities γ_s (skew angle) and γ_t (tilt angle), Figure 4. In the current work, values for the displacement terms b_x, b_y, γ_s, γ_t, with the roller speed vectors $\underline{\omega}_r$ and $\underline{\omega}_0$

(Figures 3 and 4) specify the roller response.

Cage response is described by a rotation about its x-axis, ψ, and translation in its radial plane, c_y, c_z, Figure 5. If the bearing contains a split (two piece) cage, Figure 6, each half of the cage is permitted three degrees of freedom. The vector

$$\underline{X} = (b_x,\ b_y,\ \gamma_s,\ \gamma_t,\ |\underline{\omega}_r|,\ |\underline{\omega}_0|)^i,\ \psi,\ c_y, c_z,\ a_x,\ a_y,\ a_z$$

$$i = 1, 2, \ldots, n_t$$

is the vector of unknowns and contains the bearing independent variables. Their values describe the bearing's response to a given set of operating conditions.

Values for the independent variables are obtained as follows. First, field equations of force and moment static equilibrium are formulated for bearing components (rollers, cage and inner ring) in terms of their displacements and speeds. Constant quantities in the field equation set characterize bearing geometry, material properties and specific operating conditions.

Because equations of static equilibrium are applied in the presence of acceleration, quasidynamic forces and moments (see page .5) are included to account for the effects of such transient loading.

A modified Newton-Raphson iterative numerical method is used to obtain the unique set of solution values for the independent variables.

These values in turn enable the computation of derived quantities, such as heat generation rate and fatigue life.

2.1 Preliminary Computations

A substantial amount of computation time can be saved if those terms which are not functions of the independent variables are evaluated prior to entering iterative solution loops. Terms, such as pitch diameter, are therefore computed once and then stored for later use. Computation details having practical importance in the analysis are discussed below.

Changes in shaft/inner-ring and outer-ring/housing fit pressures are computed as a function of the initial interference, operating temperatures and speed. The changes in diametral clearance, from off-the-shelf to operating value, are evaluated as functions of operating fit pressures and, both, thermal and rotation-induced radial growth [13].

Lubricant properties at the operating temperatures are evaluated once. Density is computed relative to a reference value at 16°C (60°F)

$$\rho = \rho_{16} - G\ (T_c - 16) \tag{1}$$

Kinematic viscosity (ν) at atmospheric pressure is obtained from Walther's equation [14].

$$\log_{10} \log_{10} (\nu + .6) = A^* - B^* \log_{10} (1.8T_c + 492) \tag{2}$$

Dynamic viscosity is given by:

$$\eta_0 = (9.8 \times 10^{-3})\ \rho\nu \qquad (3)$$

The pressure viscosity coefficient is computed from a relation developed by Fresco [15].

$$\alpha = (3.3403 \times 10^{-8})\ [C^* + D^*\log_{10}\nu + E^*(\log_{10}\nu)^2]^{\left(\frac{560}{1.8T_c+492}\right)} \qquad (4)$$

Values for constant terms in equations (1) through (4), for two lubricants, are given in Table 1.

2.2 Development of Mathematical Bearing Models

The equilibrium field equation set, a global mathematical model, is formulated by summing the loads contributed by specific local forces. Figure 7 shows those forces which have been considered in the analysis to act on a roller. Details of the mathematical models used to compute them follow.

Roller to raceway contact elastic load is computed to recognize the influence of material properties, geometry, and component displacement. Given a set of values for the independent variables, component locations are established in space. Assuming Hertzian contact, and using the slicing technique [16], relative positions of the rollers and rings are examined at each slice to determine if bodies contact or if free space exists between them. Relative position is established by using standard coordinate frame transformations

[17].[3] Locations and magnitudes of interpenetration are recorded, with consideration for change in clearance, and well established equations [7] are used to determine maximum contact stress (σ), contact half width (b), elastic force ($\underline{F}$) and moment ($\underline{M}$).

Roller to raceway contact friction loads (fo and f_I) are computed as functions of position and speed. Let $\underline{p}$ be a vector locating a slice contact point, then the velocity of the roller surface at this point, relative to an observer moving at speed $\underline{\omega}_0$, is:

$$\underline{v}_1 = \underline{\omega}_r \vec{x}\ \underline{p} \tag{5}$$

The velocity of the raceway surface at the same point is:

$$\underline{v}_2 = (\underline{\omega}^* - \underline{\omega}_0) \vec{x}\ \underline{p} \tag{6}$$

where $\underline{\omega}^* = 0$ for outer raceway contacts and $\underline{\omega}^* = \underline{\omega}$ for inner raceway contacts. Equations (5) and (6) enable computation of the sliding and entrainment velocities

$$\underline{V} = \underline{v}_2 - \underline{v}_1 \tag{7}$$

$$\underline{U} = 1/2(\underline{v}_1 + \underline{v}_2) \tag{8}$$

EHD film thickness is computed at each slice using the Loewenthal [18] model:

---

[3]See Appendix A - "Coordinate Frame Definitions and Transformations".

$$h_0 = K_L\,(\rho')^{-1}\,(\eta_0|\underline{U}|\rho'/E)^{.62}\,(\sigma/E')^{-.22}\,\phi_S \tag{9}$$

Lubricant inside the concentrated contact will be exposed to a shear stress proportional to sliding speed. Assuming Newtonian fluid, linear velocity gradient, and exponentially varying fluid viscosity, the Allen [19] traction model is used to obtain shear stress as

$$\tau = \eta_0\,\exp(\alpha\sigma)\,\left(\frac{V_{2z} - V_{1z}}{h_0}\right) \tag{10a}$$

or

$$\tau = f_A\sigma \quad \begin{array}{l} \text{when } \eta_0\,\exp(\alpha\sigma)\left(\dfrac{V_{2z} - V_{1z}}{h_0}\right) > f_A\sigma \\ \text{and } \eta_0\,\exp(\alpha\sigma)\left(\dfrac{V_{2z} - V_{1z}}{h_0}\right) > \tau_c \end{array} \tag{10b}$$

The magnitude of the contact friction force, $|\underline{f}|$, is evaluated by integrating the shear stress, equation (10), over the contact area. Integration is performed using Simpson's Rule, assuming uniform velocity over the slice contact area and a semicylindrical pressure distribution. The friction force vector is directed along the sliding velocity vector

$$\underline{f} = |\underline{f}|\,\frac{\underline{V}}{|\underline{V}|} \tag{11}$$

The moment generated by friction is given by

$$\underline{m} = \underline{p} \stackrel{\rightarrow}{x} \underline{f} \tag{12}$$

Heat generation rate is taken as the thermal equivalent of mechanical work.

$$\dot{q}_1 = \underline{f} \cdot \underline{V} \tag{13}$$

F-4185C-1-R100

The EHD film starts in a gently narrowing inlet region where lubricant is entrained into the contact, Figure 7. Pressure builds up gradually in this hydrodynamic inlet, adding to rolling resistance. Computation of the net hydrodynamic force ($\underline{h}$) and moment ($\underline{t}$) is performed using the methods presented by Floberg [20] and Chiu [21]. Both cavitation and starvation are considered.

Roller end to flange load computation is similar to that made for the raceway. Independent variable values are used to establish, by coordinate transformation, the relative position of rollers with respect to the flange. Contact point location ($\underline{p}_f$) and penetration magnitude (δ_f) are computed in closed form [22].

The roller end to flange contact area, for sphere-ended rollers against an angled flange, can take on three possible shapes for a given load:

(1) The contact area is Hertzian and elliptical in shape for relatively small end sphere radii over a limited, but practical, extent of roller to flange positions.

(2) As end radius is increased, the contact area increases to a size bounded by the finite dimensions of the flange and roller end, producing high stresses at the boundaries.

(3) When the sphere radius is large, the roller end may touch the flange at two non-Hertzian

contact points.

Type (1) Hertzian point contact has been shown, by experiment [23], to be desirable because of its high load carrying capacity and ability to form a lubricant film.

In the current work, Hertzian point contact at the flange is assumed. Contact maximum stress (σ_f) and dimensions (a_f, b_f) are evaluated as functions of geometry, material properties and load [7].

After a program execution, an examination of predicted contact dimensions and contact point locations enable the determination if type (1) Hertzian contact exists. Subsequent executions can be made to select roller and/or flange geometries which provide this condition.

The roller end to flange contact force ($\underline{f}_f$) is set so that the magnitude of its axial component, f_{fx}, provides roller axial equilibrium. The f_{fy} and f_{fz} components of $\underline{f}_f$ are computed as a function of sliding and entrainment velocities at the contact point $\underline{p}_f$. Both EHD and inlet region HD force components are considered [19,20,21]. Computation of sliding and entrainment velocities is accomplished by using the point $\underline{p}_f$ in place of $\underline{p}$ in equations (5) through (8).

Moment ($\underline{g}_f$) is computed from the vector cross product $\underline{p}_f \vec{x} \underline{f}_f$, and heat generation rate is taken as the thermal equivalent of mechanical work

$$\dot{q}_2 = \underline{f}_f \bullet \{ (\underline{\omega} - \underline{\omega}_0) \vec{x} \; \underline{p}_f - (\underline{\omega}_r \times \underline{p}_f) \} \qquad (14)$$

<u>Quasidynamic roller loading</u> has been included to apply the equations of static equilibrium in the presence of acceleration. Four specific terms are considered here. Roller centrifugal force ($\underline{\dot{C}}$) and the gyroscopic moment ($\underline{G}$) vectors are evaluated as functions of roller position and speeds [24]. The two additional terms, included to reflect the inertial forces imposed during changes in roller orbital and rotational velocities, are given by Kellstrom [25] as

$$\underline{F}_q = \frac{Mn}{8\pi} |\underline{\omega}_0|^{i} \; D_{AVG} \; [|\underline{\omega}_0|^{i+1} - |\underline{\omega}_0|^{i-1}] \; \hat{k} \qquad (15)$$

$$\underline{M}_q = \frac{MnD^2}{32\pi} \; |\underline{\omega}_0|^{i} \; [\, |\underline{\omega}_r|^{i+1} - |\underline{\omega}_r|^{i-1} \,] \, \hat{i} \qquad (16)$$

where D_{AVG} is the bearing's pitch diameter.

<u>Roller drag</u> is included to account for forces generated when the lubricant is churned as it passes through the bearing cavity. The analytic description of roller drag presented here is obtained from equations describing external flow over a cylinder [26].

$$\underline{D} = -9.8 \times 10^3 \; (\rho\zeta) \; \frac{D^2_{AVG} C_D l e^D}{8} \; (\underline{\omega}_0 \bullet \underline{\omega}_0) \; \hat{k} \qquad (17)$$

The term $\rho\zeta$ in equation (17) is the effective density of the air-oil mixture in the bearing cavity, and must be chosen to reflect bearing operating conditions. Correlation of experimental data with program predicted results [27,12], for a 40 mm jet lubricated spherical bearing, has shown ζ lies in the range

$$.01 \leq \zeta \leq .02$$

for shaft speeds to 5000 rpm. It is expected that this range of values would be valid at higher speeds also. Note that because spherical roller bearings are typically operated at low speeds, the drag force is also very low. The 40mm bore spherical roller bearing operating at 5000 RPM, for example, will experience a drag of .3N (.07 lbs) per roller for $\zeta = 0.02$.

Roller to cage pocket contact load is a function of lubricant properties, speed, geometry and the position of the roller within the pocket. In the current work, the cage pocket geometry is taken as a rectangular cavity.

It has been shown [3] that under typical operating conditions, skew moments (moment loading about the $y_{\bar{R}}$ axis, Figure 4) are imposed on the roller at both the outer and inner raceway contacts. Depending upon the magnitude of the skew moments, one of the following situations can occur:

(1) The roller skews about the $Y_{\bar{R}}$ axis by some small amount. This is sufficient to balance the raceway induced moments with negligible assistance from the cage pocket or flange.

(2) The roller continues to skew past

the above condition until raceway induced moments are balanced by mutual contributions from the flange and cage pocket.

(3) The bearing is manufactured without an integral flange. The roller continues to skew past the condition in (1), until equilibrium is achieved through balance of raceway and pocket induced moments.

For the analytic assessment of pocket-induced skew moments, it is assumed that loads are sufficiently light to produce hydrodynamic contact, and that the pocket is fully flooded with lubricant. The slicing technique is then used to evaluate the forces and moments generated at the various stations along the skewed roller-to-pocket contact.

In [28], it was shown that roller position within the cage pocket could be written in terms of the roller's speed and cage speed. Assuming the cage speed vector, $\underline{\omega}_c$, is coincident with the centerline of the inner ring and its magnitude is the average of all roller orbital speeds, the j-th roller center to cage pocket center offset is

$$(Z)^j = \pm \frac{D_{AVG}\pi}{2n} \sum_{\ell=2}^{\ell=j} \left\{ \frac{|\underline{\omega}_0|^{\ell-1} + |\omega_0|^{\ell}}{\underline{\omega}_c} - 1 \right\} + (Z)^1 \qquad (18a)$$

$j = 2, 3, \ldots, n$

where

$$(Z)^1 = \pm 1/2\ D_{AVG} \sin \Psi \pm c_y \sin \phi_1 \mp c_z \cos \phi_1 \qquad (18b)$$

Ψ = angular displacement of cage relative to its reference position

ϕ_1 = azimuthal angle of first roller

c_y = cage radial displacement in y direction

c_z = cage radial displacement in z direction

Note that equation (18) is applied to each row of rollers, where the upper sign refers to row 2 and the lower sign to row 1. The minimum hydrodynamic film thickness at the leading (+) and trailing (-) edge of each slice is given by (Figure 8)

$$(h_0^+)^i = \frac{^1c}{2} - (Z)^i + \bar{x} \sin (\gamma_s)^i - r_{\bar{x}} \cos (\gamma_s)^i \qquad (19)$$

$$(h_0^-)^i = \frac{^1c}{2} + (Z)^i - \bar{x} \sin (\gamma_s)^i - r_{\bar{x}} \cos (\gamma_s)^i \qquad (20)$$

$$i = 1,2,\ldots n_t$$

where $r_{\bar{x}}$ is the radius of the slice loacated at $x = \bar{x}$.

Friction force acting on a particular slice, $(R_y)_{\bar{x}}$, is computed as a function of the normal force. Equations are used which describe the hydrodynamic lubrication of a rigid cylinder near a flat plate [29]. The normal force is obtained as a function of the film thickness, using a linear approximation of the hydrodynamic equations.

Tne heat generation rate is taken as the thermal equivalent of mechanical work

$$(\dot{q}_3)_{\bar{x}} = (R_y)_{\bar{x}} (r_{\bar{x}} |\underline{\omega}_r|) \qquad (21)$$

The sum of the individual forces acting on each slice yields the total cage pocket force ($\underline{R}$) and moment ($\underline{S}$).

Cage rail/ring land torque and forces are computed from the hydrodynamic solution for short, self acting journal bearings [30].

$$\underline{T} = \pm \frac{2\pi}{C_g} \frac{\eta_0 r_g^3 w_g}{(1-\varepsilon^2)^{1/2}} \cdot |\underline{\omega} - \underline{\omega}_c| \ \hat{i} \tag{22}$$

$$F_y = \frac{\eta_0 r_g w_g^3}{C_g^2} \cdot \frac{\varepsilon^2}{(1-\varepsilon^2)^2} \cdot |\underline{\omega} + \underline{\omega}_c| \tag{23}$$

$$F_z = \frac{\eta_0 r_g w_g^3}{C_g^2} \cdot \frac{\varepsilon}{4(1-\varepsilon^2)^{3/2}} \cdot |\underline{\omega} + \underline{\omega}_c| \tag{24}$$

Several bearing designs employ cages having multiple rails. Here, torque and radial loads are computed by specifying the rail land diameter and rail width of an equivalent single-railed cage. Dimensions are chosen so that the single rail equivalent cage and multiple rail existing cage produce identical torque and radial force at the same eccentricity values. The equivalent rail land radius is:

$$r_g = (a)/(a^3/b)^{.375} \tag{25}$$

And the equivalent rail width is:

$$w_g = (a^3/b)^{.125} \tag{26}$$

where:

$$a = \sum_{\ell = 1}^{\ell = \text{number of rails}} (rw^3)_\ell$$

$$b = \sum_{\ell = 1}^{\ell = \text{number of rails}} (r^3 w)_\ell$$

r = rail land radius of the ℓ-th rail (M)

w = the rail width of the ℓ-th rail (M)

Torque generated at the interface between split cage halves is computed by assuming a uniform pressure distribution over the interface and a constant coefficient of friction:

$$\underline{T}_s = \pm \left(\frac{B^3 - A^3}{B^2 - A^2}\right) \frac{2}{3} (Fx)\mu \tag{27}$$

Where μ is the coefficient of friction at the split, Fx is the axial load supported at the split and A and B are radii defined in Figure 9. Torque computed by (27), is directed so that the slower cage piece is accelerated and the faster cage piece is decelerated.

Heat generation rate at the split is given by:

$$q_4 = \underline{T}_s \cdot (\underline{\omega}_{c1} - \underline{\omega}_{c2}) \tag{28}$$

where $\underline{w}_{c1}$ and $\underline{w}_{c2}$ are speeds of each cage piece.

Heat generation rate at the cage rail is given by

$$q_5 = \underline{T} \cdot (\underline{\omega}_c - \underline{\omega}) \tag{29}$$

2.3 Formulation of Equation Set

The field equation set is formulated by summing the loads acting on the rollers, cage and inner ring.

Equilibrium equations for the i-th roller can be represented in vector format by 2 equations

$$\sum_{m=1}^{2} \sum_{k=1}^{n_s} [(\underline{F})^i_{k,m} + (\underline{f})^i_{k,m} + (\underline{h})^i_{k,m} + (\underline{R})^i_k] + (\underline{C})^i +$$

$$(\underline{F}_q)^i + (\underline{f}_f)^i + (\underline{D})^i = 0 \tag{30}$$

and

$$\sum_{m=1}^{2} \sum_{k=1}^{n_s} [(\underline{M})^i_{k,m} + (\underline{m})^i_{k,m} + (\underline{t})^i_{k,m} + (\underline{S})^i_k] + (\underline{G})^i +$$

$$(\underline{M}_q)^i = 0 \tag{31}$$

The cage maintains equilibrium through balance of the torques induced at the pockets, rails and split interface

$$(T_s + T_x - \frac{D_{AVG}}{2} \sum_{j=1}^{n_r} \sum_{i=1}^{n} (-1^j) \; (R_z)^i) \; \hat{i} = 0 \tag{32}$$

Note that pocket loads are assumed to act at the pitch circle, and that if a split cage design is addressed, the additional term $\underline{T}_s$ (equation (27)) is included; otherwise the term is zero. Summation of pocket and rail forces in the radial directions yields:

$$\sum_{i=1}^{i=n_t} (\underline{R}_z)_i \sin \phi_i + F_y \cos\beta - F_z \sin\beta = 0 \qquad (33)$$

$$\sum_{i=1}^{i=n_t} (R_z)_i \cos\phi_i + F_y \sin\beta + F_z \cos\beta = 0 \qquad (34)$$

β is an angle measured CCW positive from the Y_c axis to the point of closest approach between the cage rail and ring land.

Three inner ring equations of force equilibrium are represented by the vector

$$\sum_{i=1}^{n_t} \sum_{k=1}^{n_s} [(\underline{F})^i_{k,2} + (\underline{f})^i_{k,2} + (\underline{h})^i_{k,2}] + (\underline{f}_f)^i + (\underline{P}) = 0 \qquad (35)$$

where $\underline{P}$ = cage-land force vector for inner ring riding cage

2.4 Computation of Planet Bearing Performance

In the calculation of roller bearing performance it was assumed that the bearing rings are rigid and that elastic deformation occurs only at the Hertzian contact. In some special cases, such as planetary gear applications, flexibility of the outer ring must be taken into account in calculating the deflection at each roller location [6].

A typical, two row spherical planet bearing is shown in Figure 10. Note that the outer ring is integral with the gear to minimize component weight.

Load is applied to the bearing at the (gear) pitch radius through diametrically opposed meshes, Figure 11. The bearing assembly maintains equilibrium by balancing the gear tooth loads with a reactive load at the carrier post.

The roller to outer ring contact loads and gear mesh loads will tend to deform the normally circular shape of the outer ring. The deformed shape can be computed by superposing the influence of each individual component of applied load. The method is described in [6], and requires that the gear mesh load, F, be represented by an equivalent set of loads applied at the outer ring neutral axis (Figure 12):

$$R = F \sin \alpha$$
$$T = F \cos \alpha$$
$$M = F\ (R_p - R_N) \cos \alpha$$

Assuming the deflections are elastic, the radial deformation of the outer ring (measured as a displacement from the neutral axis) at the i-th roller location is

$$\Delta_i = \Delta_i^M + \Delta_i^T + \Delta_i^R + \Delta_i^P \tag{37}$$

where:

$\Delta_i^M, \Delta_i^T, \Delta_i^R$ - are the outer ring deformations due to moment, tangent and radial components of gear tooth load [29], measured positive inward at the i-th rolling element location.

Δ_i^P - is the outer ring deformation due to rolling element loads, measured positive inward at the i-th rolling element location.

The roller induced ring deformations can be written as

$$\Delta_i^P = \sum_{j=1}^{n} C_{ij} P_j \tag{38}$$

Where C_{ij} are influence coefficients[4] for the outer ring and can be found in the literature [31] and P_j is the total roller to outer ring contact load of both rows at roller position j.

Inserting (38) into (37) and rearranging terms, we obtain a set of i equations describing the deformed shape of the outer ring

$$0 = (\Delta_i^M + \Delta_i^T + \Delta_i^R) + \sum_{j=1}^{n} C_{ij} P_j - \Delta_i \tag{39}$$

Equation (39) is in a form which may be solved for deflections Δ_i, using the Newton-Raphson scheme[5]. Note that

[4] The influence coefficients C_{ij} are defined as the inward deformation of the ring at i due to an outward unit load at j.

[5] When analyzing a spherical planet bearing, SPHERBEAN will formulate a set of deflection equations (39) and solve for Δ_i along with the equations describing inner ring, roller and cage equilibrium, (30) through (35).

the loads P_j are non-linear functions of Δ_i, therefore equation (39) is non-linear. Also, in those kinematic cases where the carrier is moving, the additional centrifugal load on the rolling elements must be included in P_j, Figure 13.

The rolling element centrifugal load resulting from carrier rotation is computed by transforming the roller CG coordinates to a reference frame located along the sun gear center line. This enables computation of the centrifugal force vector, which is added to the centrifugal load due to roller orbital speed.[6]

2.5 Numerical Solution to the Formulated Bearing Analysis

In contrast to the generality maintained in the bearing analysis formulation, specific solution procedures are required to address the specific problems arising during the iterative solution to equations (30) through (35) and (39).

An automated field equation set partitioning scheme was developed so that the convergence characteristics of several different subsets of equations and variables could be determined for a given load condition (i.e. pure thrust, pure radial or combined load). A table containing 12 subsets which showed most rapid convergence was coded into the SPHERBEAN. Upon execution, SPHERBEAN examines the applied load to determine

---

6 When analyzing planet bearings, "SPHERBEAN" will modify rolling element, cage and inner ring equilibrium equations to include proper centrifugal force.

direction and possible symmetries, and a corresponding pattern of equation subsets are selected from the table and sequentially brought to equilibrium using the Newton-Raphson method.

Partial derivatives, required at each iteration of the Newton-Raphson method, are computed by fitting a second order polynomial through current and two adjacent function value points, and evaluating the derivative directly from the polynomial. Although more time consuming than Newton's forward difference operator, this procedure is employed to smooth the piecewise continuity of the field equation set and provide more reliable code performance.

The numerical procedure is stopped when the RMS residual of all equations is less than a specified tolerance. Completion of the iterative procedure permits the display of values for the vector of unknowns, bearing heat generation rates and the computation of bearing fatigue life.[7] The latter is computed according to standard Lundberg-Palmgren methods [32,33], and includes correction for the dependence of life on the film thickness to surface roughness ratio [34,35].

---

[7] Fatigue life computation details are given in Appendix B.

3.0 COMPUTATION OF SYSTEM STEADY STATE AND TIME TRANSIENT THERMAL PERFORMANCE

Description to this point has addressed the bearing analysis at a given set of component temperatures. Thermal effects can be computed in either of two modes.

The first mode details the steady state operating temperatures of the bearing and its environment. SPHERBEAN will formulate the conservation of energy equations for an equivalent nodal model of the bearing and surrounding hardware. Energy equations contain heat sources which may be provided by the user to represent the heat generated at sources other than the spherical bearing, such as neighboring seals or gears. Energy equations will also contain the heat generated by the spherical roller bearing, (for example, see equations (13) and (14)). The Newton-Raphson solution method is used to solve the non-linear[8] conservation of energy equations for system temperatures. Resulting system temperatures are then used to compute bearing performance, including bearing heat generation rate. This iterative procedure, shown in Figure 14, is stopped when the difference between current and previous temperature predictions is less than a user specified tolerance (typically set at $2^{\circ}C$).

[8]The equation set is non-linear because it contains terms describing radiation and free convection (see Appendix C).

The second mode can be used to detail <u>time transient thermal performance</u> of the bearing and its environment. Here, SPHERBEAN will formulate and solve a system of first order nonlinear differential equations. Typically, initial values are taken as the solution to a steady state analysis.

A detailed description of both steady state and time transient analysis can be found in Appendix C and in Volume II [11] of this work.

4.0 CONCLUSIONS AND RECOMMENDATIONS

The material presented in the preceeding sections documents the creation of the state of the art spherical bearing analysis/ design tool SPHERBEAN. The formulations are general and the program architecture modular to permit easy maintenance and expansion.

During the course of the work performed, a perspective was gained on the additional requirements for the accurate simulation of spherical roller bearing performance.

Proper assessment of performance demands an investment in basic formulation and corresponding detailed experimental verification. It is specifically recommended that:

1. The EHD traction and film thickness models be upgraded to include effects of surface micro-geometry. Because spherical roller bearings are typically operated at low speed, EHD film thickness at roller-to-raceway contacts will likely be several times less than the composite surface roughness in typical spherical bearing applications.

2. The effects of lubricant application rate and distribution within the bearing cavity be investigated. Thermal dimensional stability is sensitive to the assumptions concerning the lubricant distribution within the bearing cavity (ξ), and the sensitivity is accentuated with increased speed.[9]

[9] See Example 1 in Volume II.

Since spherical roller bearings are being asked to follow the DN capabilities of ball, cylindirical and tapered roller bearings, realistic assessment of their high speed performance requires an accurate method of relating drag power loss to lubricant application rate.

3. In light of the low film thickness to surface roughness ratios (Λ) that spherical roller bearings typically operate under, surface traction effects should be directly related to material failure and thus bearing failure predictions.

4. The kinematic description of inner ring displacement should be expanded to include a misalignment angle, and the performance of misaligned spherical roller bearings with outer ring rotation be fully examined.

5.0 LIST OF REFERENCES

1. Harris, T. A., "The Effect of Misalignment of the Fatigue Life of Cylindrical Roller Bearings Having Crowned Roller Members," ASME Journal of Lubrication Technology, Vol. 91, No. 2, April 1969, pp. 294-300.

2. Pirvics, J., "The Analysis of Thermal Effects in Rolling Element Bearing Load Support Systems," Proceedings of the 6th Leeds/Lyon Symposium on Tribology at Lyon, September 1979.

3. Kellstrom, E. M., "Rolling Contact Guidance of Rollers in Spherical Roller Bearings," Presented at Joint ASME/ASLE Lubrication Conference, Dayton, Ohio, October 1979, ASME paper 79-LUB-23.

4. Wieland, W. P., and Poesl, W., "State of the Art in Spherical Roller Bearings," presented at the Off-Highway Vehicle Meeting and Exposition, MECCA, Milwaukee, September 1979, SAE Paper No. 790850.

5. Harris, T. A., and Broschard, J.L., "Analysis of an Improved Planetary Gear - Transmission Bearing," ASME Journal of Basic Engineering, pp. 457-462 (September 1964).

6. Liu, J. Y., and Chiu, Y. P., "Analysis of Planet Bearing in a Gear Transmission System," ASME paper No. 75-LUB-23.

7. Palmgren, A., Ball and Roller Bearing Engineering, Third Edition, Burbank, 1959.

8. Harris, T. A., Rolling Bearing Analysis, Wiley Inc., 1966.

9. Kleckner, R. J., Pirvics, J., and Castelli, V., "High Speed Cylindrical Rolling Element Bearing Analysis "CYBEAN" - Analytic Formulation," Trans. ASME, JOLT, pp. 380-390, (July 1980).

10. Crecelius, W. J., "User's Manual for Steady State and Transient Thermal Analysis of a Shaft-Bearing System (SHABERTH), Contract Report ARBRL-CR-00386, November 1978.

11. Kleckner, R. J., and Dyba, G., "SKF Computer Program SPHERBEAN - Volume II: User's Manual," SKF Report No. AT81D007, Submitted to NASA/Lewis Research Center under NASA Contract No. NAS3-20824, NASA CR-165204 (December 1980).

12. Kleckner, R. J., and Rosenlieb. W. J., "SKF Computer Program SPHERBEAN - Volume III: Correlation with Full Scale Hardware Tests", SKF Report No. AT81D008, Submitted to NASA/Lewis Research Center under NASA Contract No. NAS3-20824, NASA CR-165205 (December 1980).

13. Timoshenko, S., Strength of Materials - Part II, Third Edition, Van Nostrand, 1958.

14. McGrew, J. M., et al, "Elastohydrodynamic Lubrication Preliminary Design Manual," Technical Report AFAPL-TR-70-27, pp. 20-21, November 1970.

15. Fresco, G. P., et al., "Measurement and Prediction of Viscosity-Pressure Characteristics of Liquids," A Thesis in Chemical Engineering Report No. PRL 3-66, Dept. of Chemical Engineering, College of Engineering, The Penna. State University, University Park, Pa.

16. Harris, T. A., "Misaligned Roller Bearings," Machine Design, pp. 98-101. August 29, 1968.

17. Goldstein, H., Classical Mechanics, Addison-Wesley, 1965, pp. 93-109.

18. Loewenthal, S. H., Parker, R. J., and Zaretsky, E. V., "Correlation of Elastohydrodynamic Film Thickness Measurements for Fluorocarbon, Type II Ester and Polyphenal Ether Lubricants," NASA Technical Note D-7825, National Aeronautics and Space Administration, Washington, D.C., November 1974.

19. Allen, C. W., Townsend, D. P., and Zaretsky, E. V., "New Generalized Rheological Model for Lubrication of a Ball Spinning in a Nonconforming Groove," NASA Technical Note D-7280, National Aeronautics and Space Administration, Washington, D.C., May 1973.

20. Floberg, L., "Lubrication of Two Cylindrical Surfaces Considering Cavitation," Trans. Chalmers Univ. Tech. No. 234, Gothenberg, 1961.

21. Chiu, Y. P., "An Analysis and Prediction of Lubricant Film Starvation in Rolling Contact Systems," ASLE Trans., Vol. 17, 1974, pp. 23-35.

22. Appendix A of Reference 9: "Roller End Flange Contact."

23. Morrison, F. R., et al, "A Functional Evaluation of a Thrust Carrying Cylindrical Roller Bearing Design," Trans. ASME, JOLT, pp. 164-170, (April 1979).

24. Merium, J. L., Dynamics, Second Edition, Wiley, 1979.

25. Kellstrom, M., "A Computer Program for Elastic and Thermal Analysis of Shaft Bearing Systems," SKF Report No. AL74P004, submitted to Vulnerability Laboratory, U. S. Army Ballistics Research Laboratory, under Contract No. DAAD05-73-C-0011, (1974).

26. Hansen, A. G., Fluid Mechanics, Wiley, pp. 452-457 (1967).

27. Kleckner, R. J., Pirvics, J. and Dyba G., "Analysis of Spherical Roller Bearing Thermomechanical Performance," to be presented at the joint ASME/ASLE Lubrication Conference, New Orleans, Louisiana (October 5-7, 1981).

28. Crecelius, W. J., et al., "Improved Flexible Shaft-Bearing Thermal Analysis with NASA Friction Models and Cage Effects," SKF Report No. AL76P003 (February 1976).

29. Dowson, D., and Higginson, G. R. Elasto-Hydrodynamic Lubrication, Pergamon Press, p. 41, 1966.

30. Pinkus, O. and Sternlicht, B., Theory of Hydrodynamic Lubrication, McGraw-Hill, New York, 1961, p. 48.

31. Liu, J. Y., and Chiu, Y. P., "Analysis of a Thin Elastic Ring Under Arbitrary Loading," Journal of Engineering for Industry, ASME, TRANS., August 1974.

32. Lundberg, G., and Palmgren, A., "Dynamic Capacity of Roller Bearings," Acta Polytechnica, Vol. 1, No. 3, 1947.

33. Lundberg, G. and Palmgren, A., "Dynamic Capacity of Roller Bearings," Acta Polytechnica, Vol. 2, No. 4, 1952.

34. Kleckner, R. J., and Dyba, G., "Curve Fit for ASME's Lubrication Life Factor vs. Λ Chart," SKF Report AL79P007L (September 1979).

35. Bamberger, E. N., Harris, T. A., Kacmarsky, W. M., Moyer, C. A., Parker, R. J., Sherlock, J. J., and Zaretsky, E. V., "Life Adjustment Factors for Ball and Roller Bearings," 1971, ASME Engrg. Design Guide.

36. Jakob, M. and Hawkins, G. A., "Elements of Heat Transfer," Third Ed., John Wiley & Sons, Inc., 1957.

37. Dusinberre, G. M., "Numerical Analysis of Heat Flow," McGraw-Hill Book Co., 1949.

38. General Electric Heat Transfer Data Book, G. E. Company, Corporate Research and Development, Schenectady, N.Y. (1976).

39. Kent's Mechanical Engineering Handbook - Power Volume, John Wiley & Son, Inc., 12th Edition, 1960, Chapter 3, p. 20.

40. Burton, R. A. and Staph, H. E., "Thermally Activated Seizure of Angular Contact Bearings," ASLE Trans. 10, pp. 408-417 (1967).

	ρ_{16} [a]	G [a]	A* [a]	B* [a]	C* [b]	D* [b]	E* [b]	ASTM SLOPE [c]
MIL-L-7808G	0.953	7.09×10^{-4}	10.215	3.698	0.0388	0.437	-0.0580	.740
MIL-L-23699	1.010	7.45×10^{-4}	10.207	3.655	0.0396	0.423	-0.0538	.731

a - From Reference [23]

b - From Reference [13]

c - ASTM Slope = .2B*

TABLE 1: Values for constant terms used in lubricant property models, Equations (1) through (4)

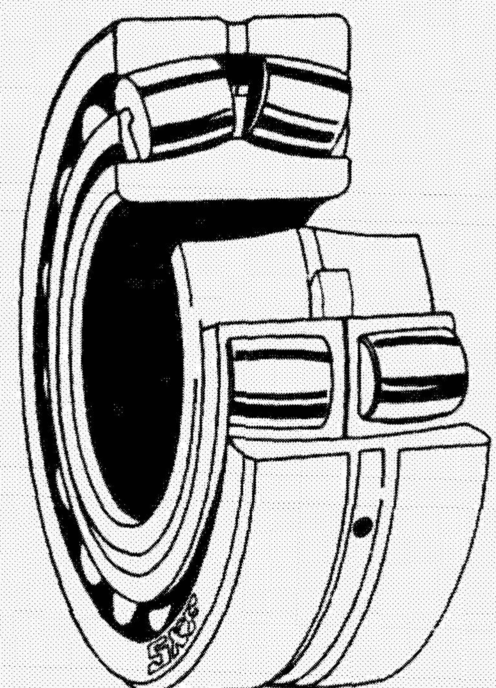

FIGURE 1 - SPHERICAL ROLLER BEARING

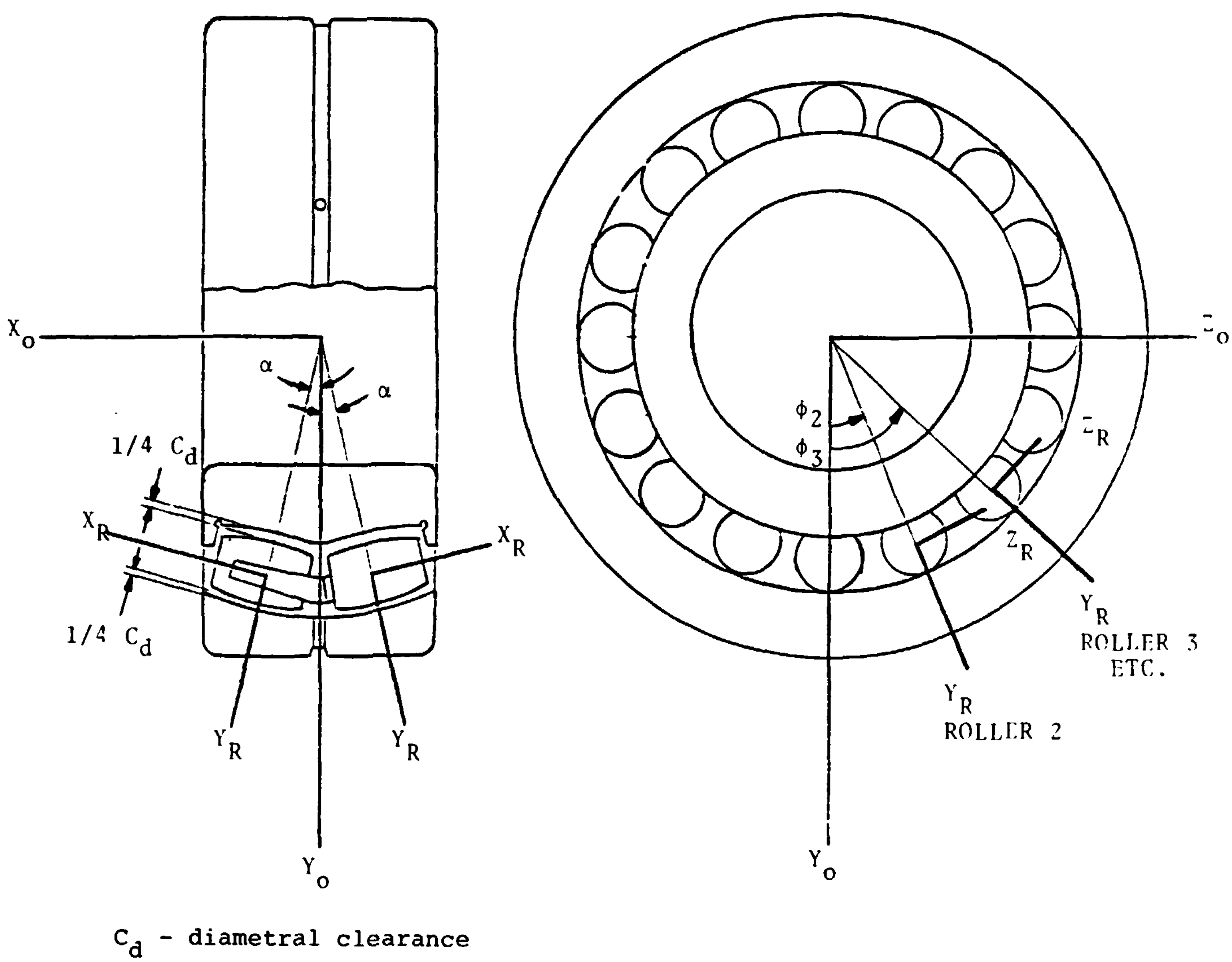

FIGURE 2: SPHERICAL ROLLER BEARING GEOMETRY
AND COORDINATE FRAMES

AT81D006

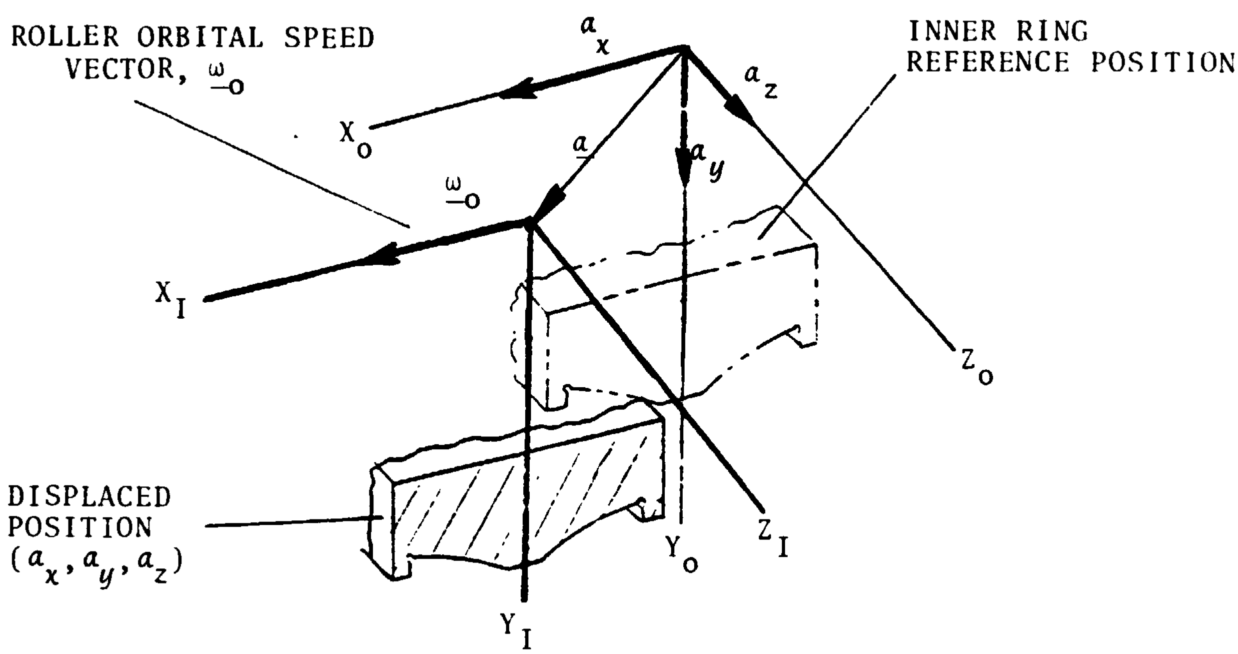

FIGURE 3: INNER RING DISPLACEMENT

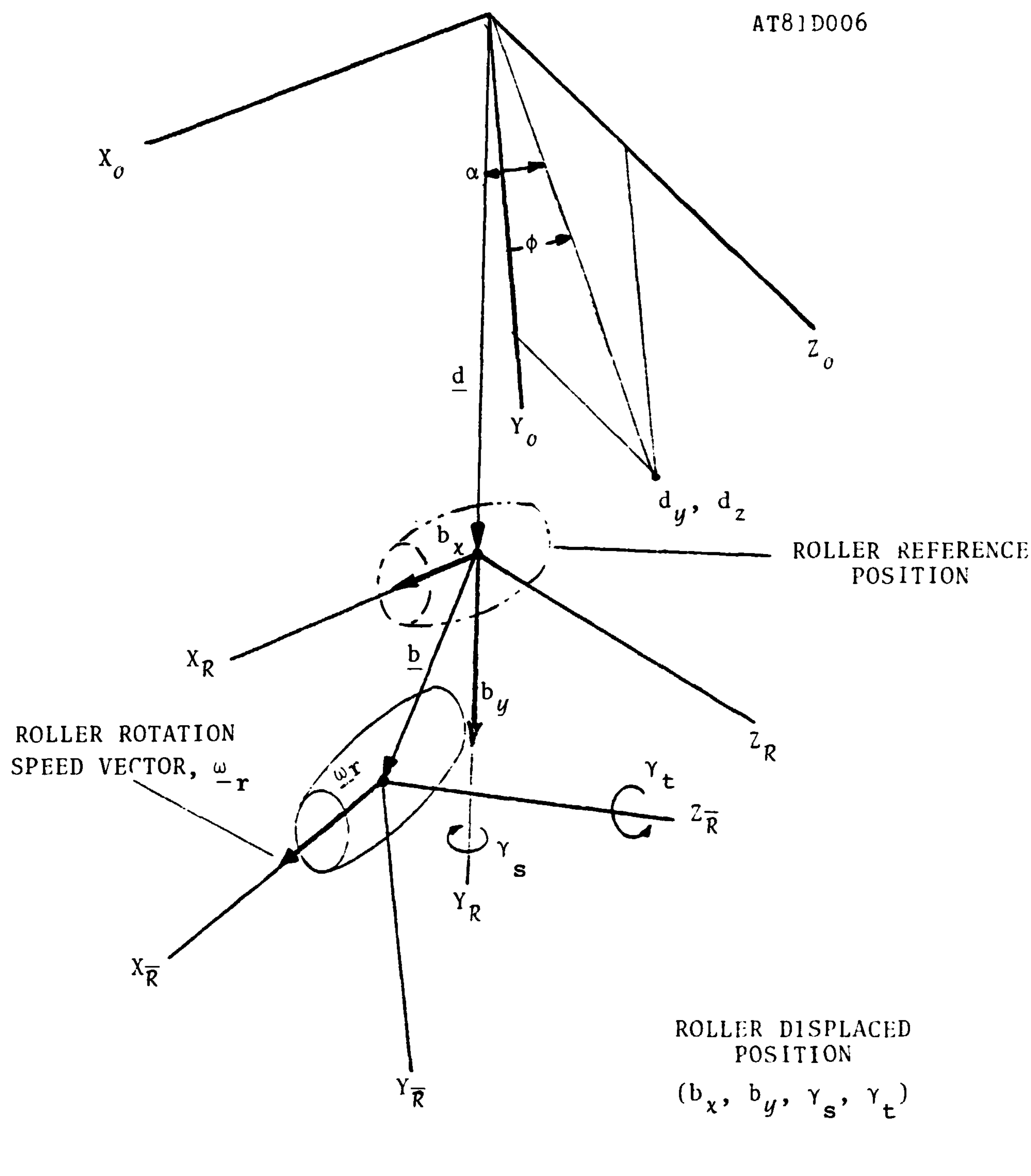

FIGURE 4: ROLLING ELEMENT DISPLACEMENT

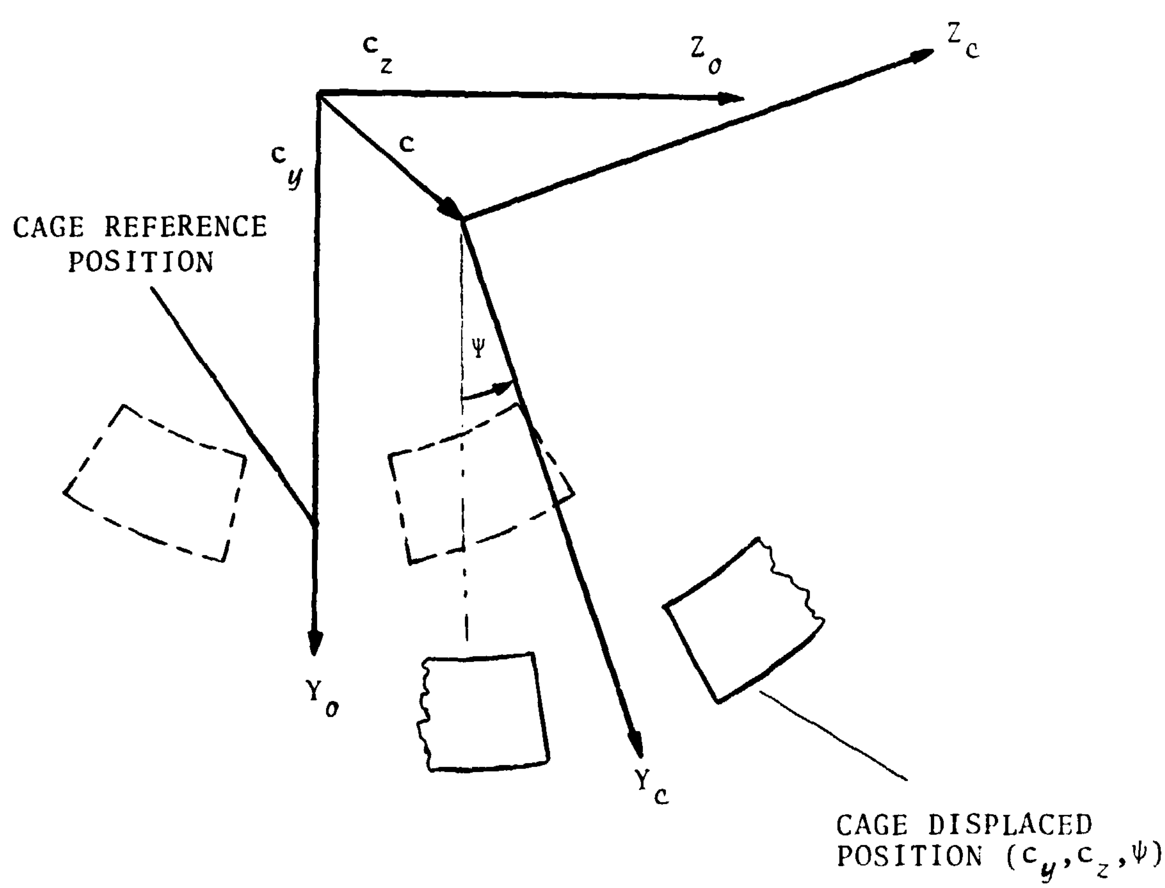

FIGURE 5: CAGE DISPLACEMENT

AT81D006

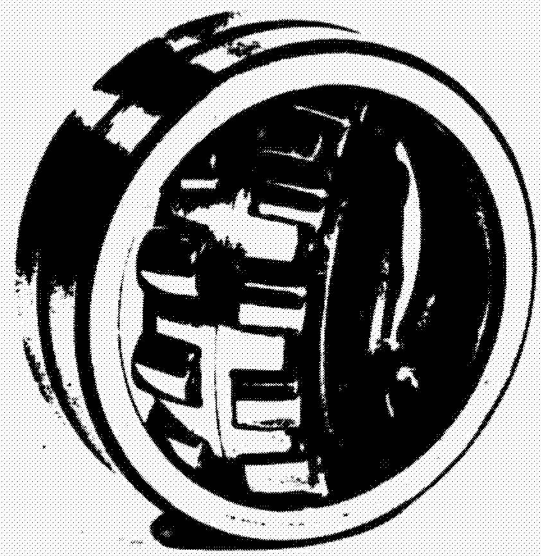

ORIGINAL PAGE
BLACK AND WHITE PHOTOGRAPH

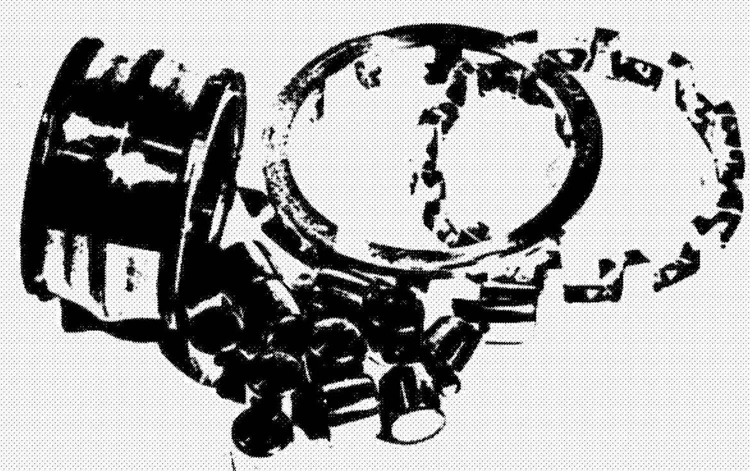

FIGURE 6: SPHERICAL ROLLER BEARING
WITH A SPLIT CAGE

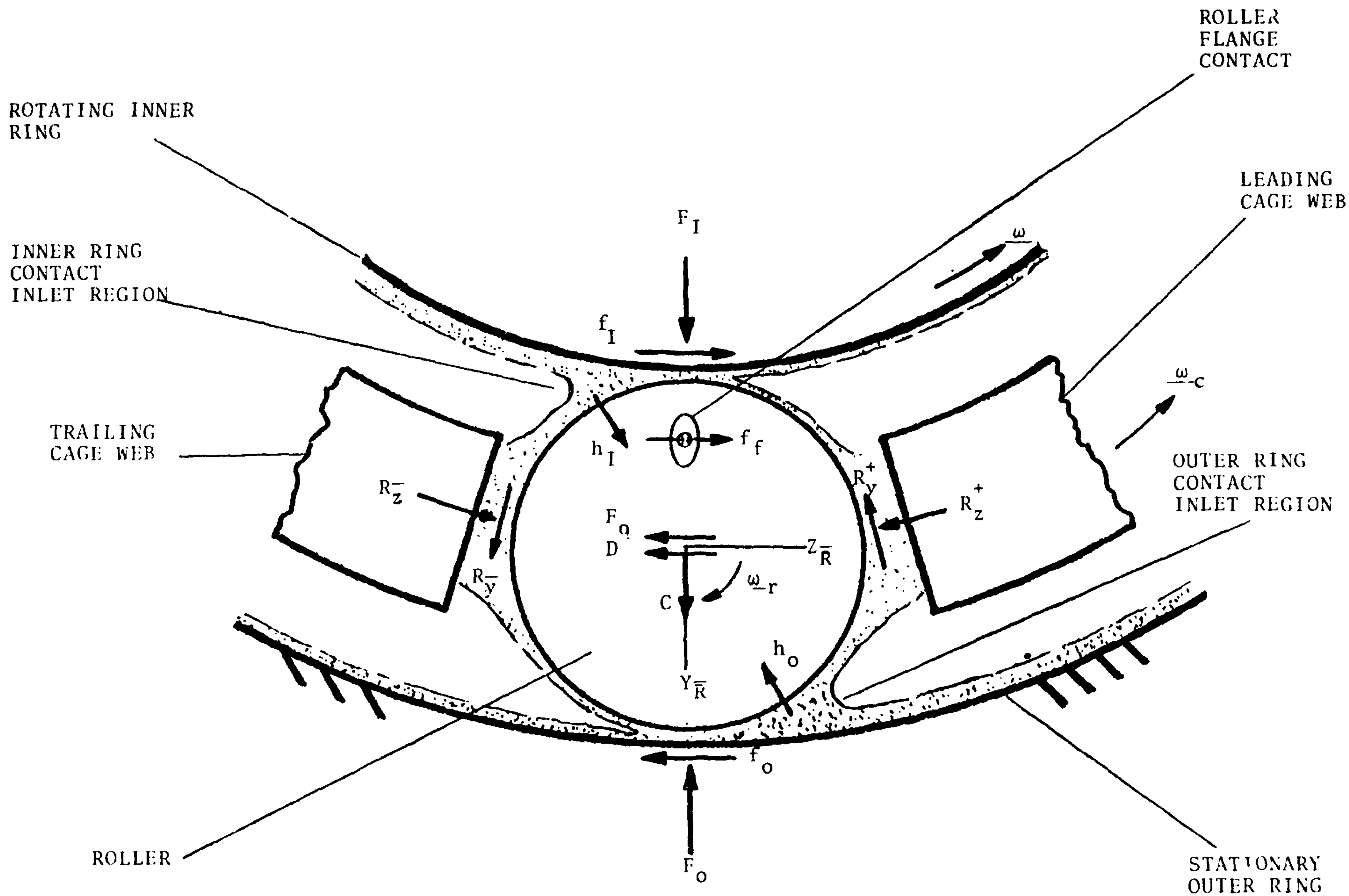

FIGURE 7: FORCES ACTING ON A ROLLING ELEMENT

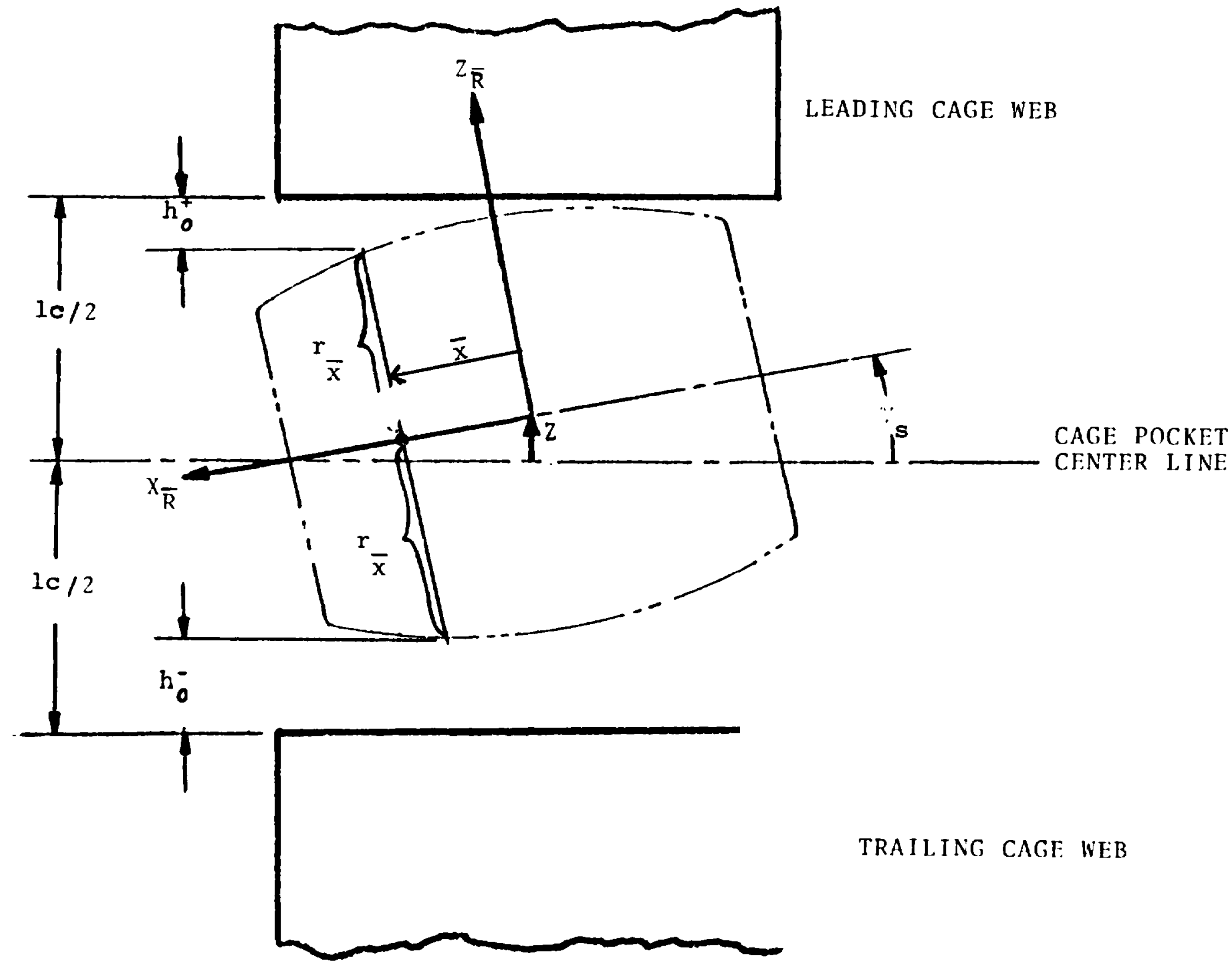

AT81D006

FIGURE 8: ROLLER TO CAGE POCKET INTERACTION

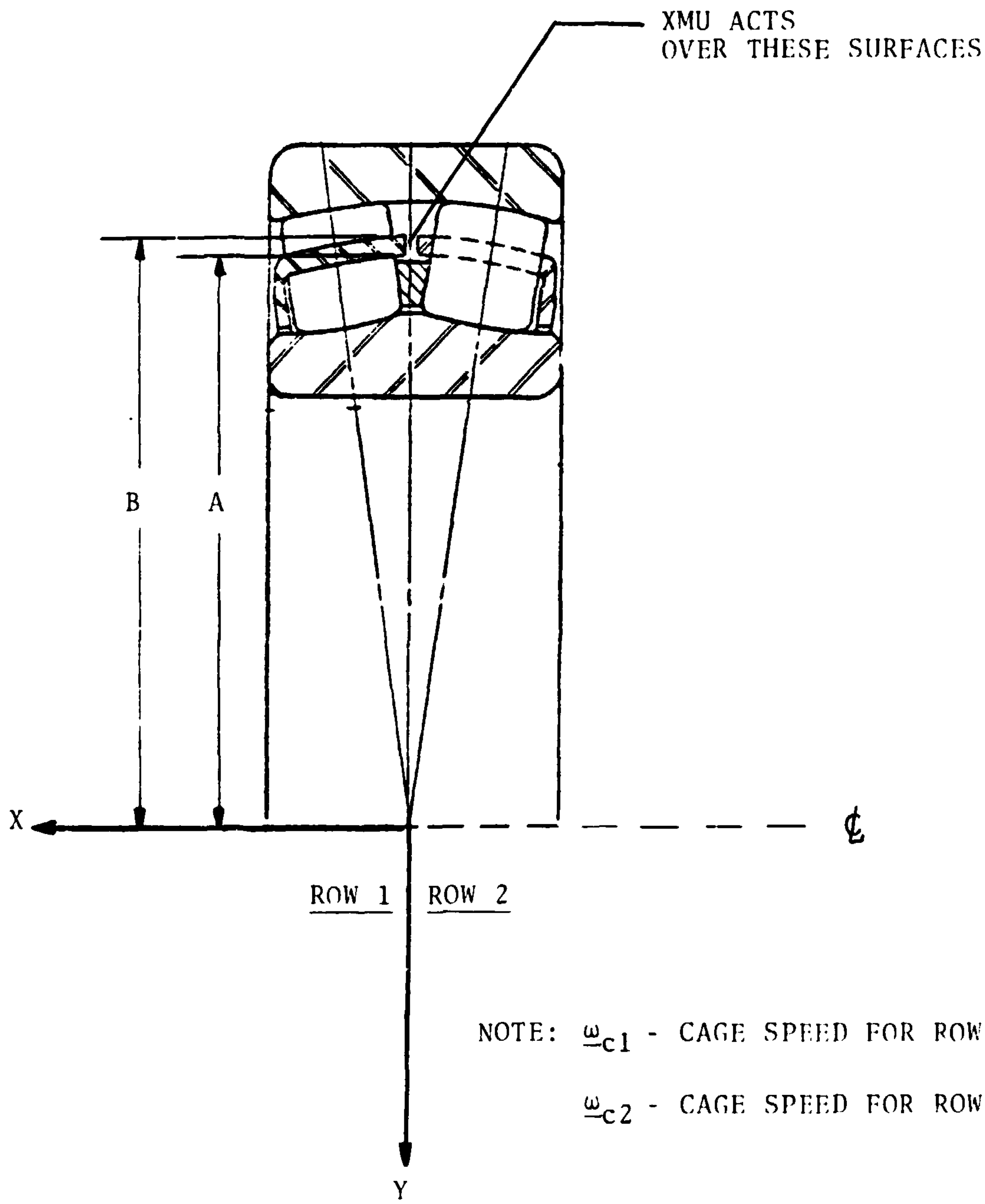

NOTE: $\underline{\omega}_{c1}$ - CAGE SPEED FOR ROW 1

$\underline{\omega}_{c2}$ - CAGE SPEED FOR ROW 2

FIGURE 9: SPLIT CAGE GEOMETRY

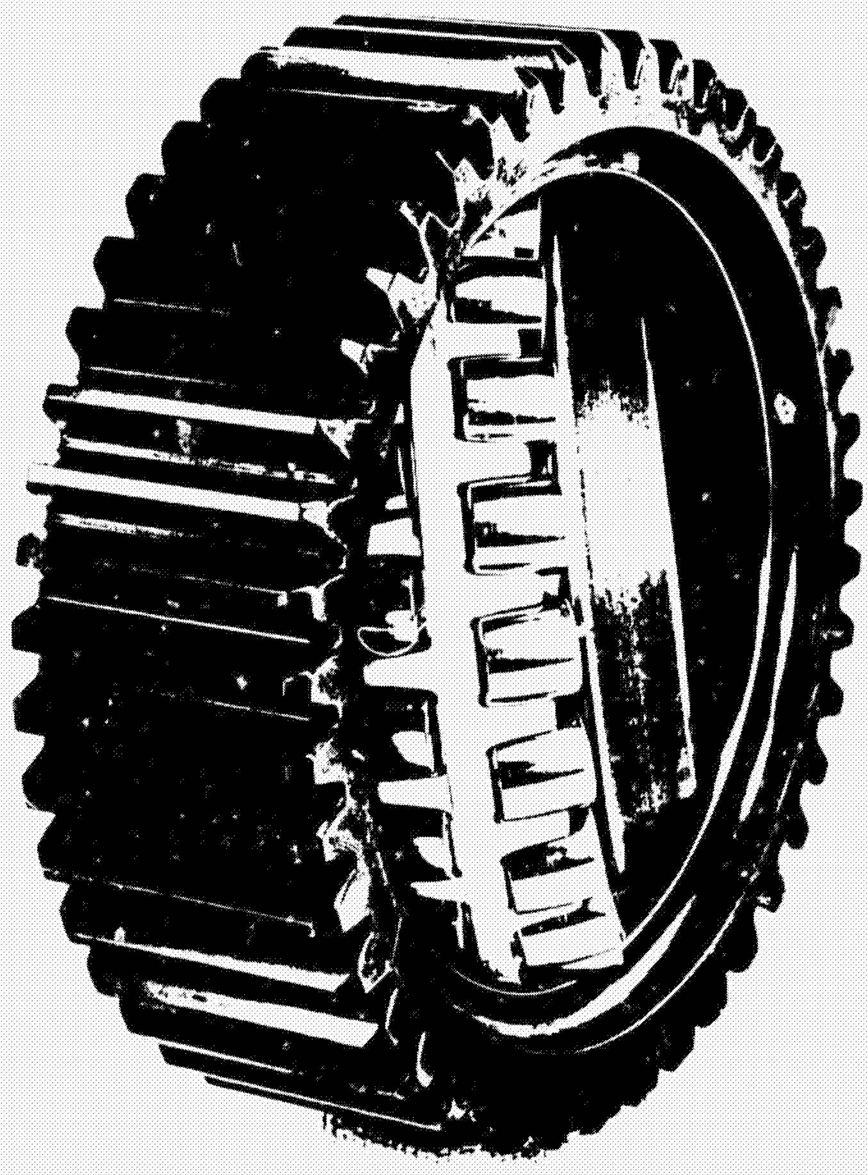

FIGURE 10: PLANET GEAR BEARING

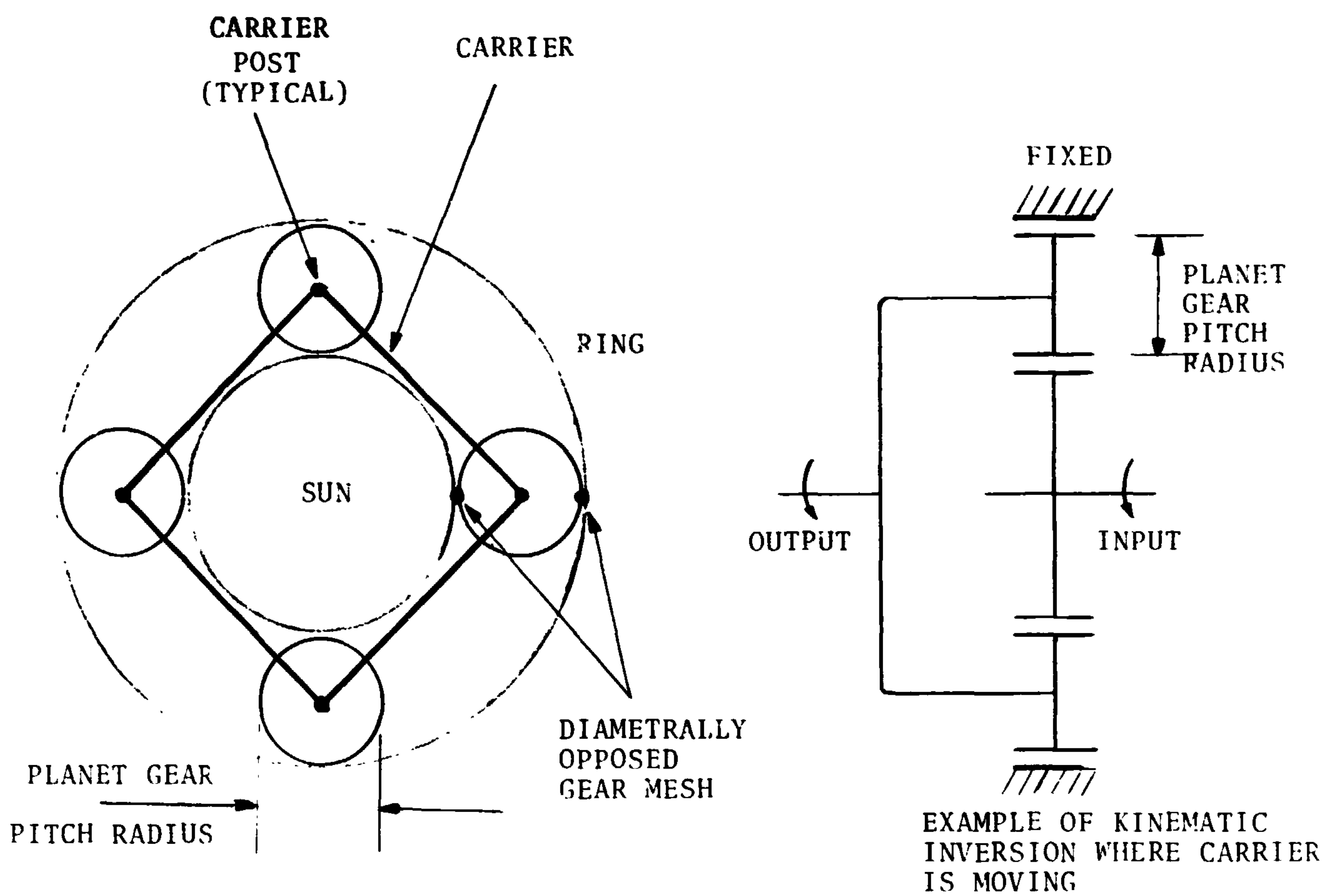

FIGURE 11: PLANETARY TRANSMISSION

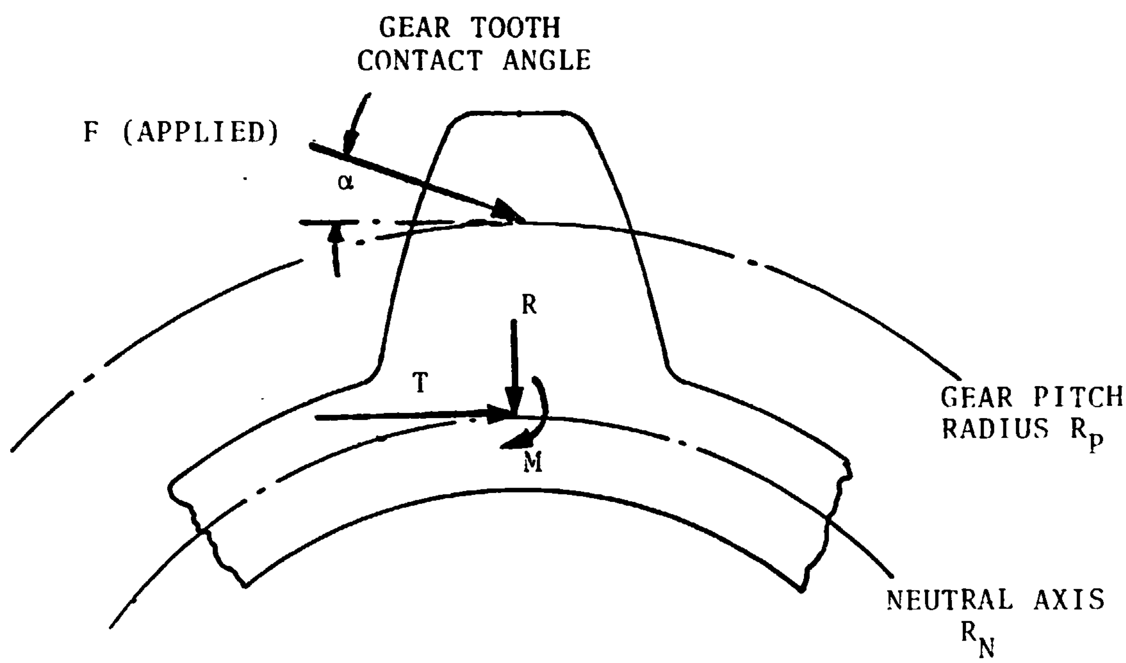

$$R = F \sin \alpha$$

$$T = F \cos \alpha$$

$$M = F (R_P - R_N) \cos \alpha$$

FIGURE 12: IDEALIZED GEAR LOADS

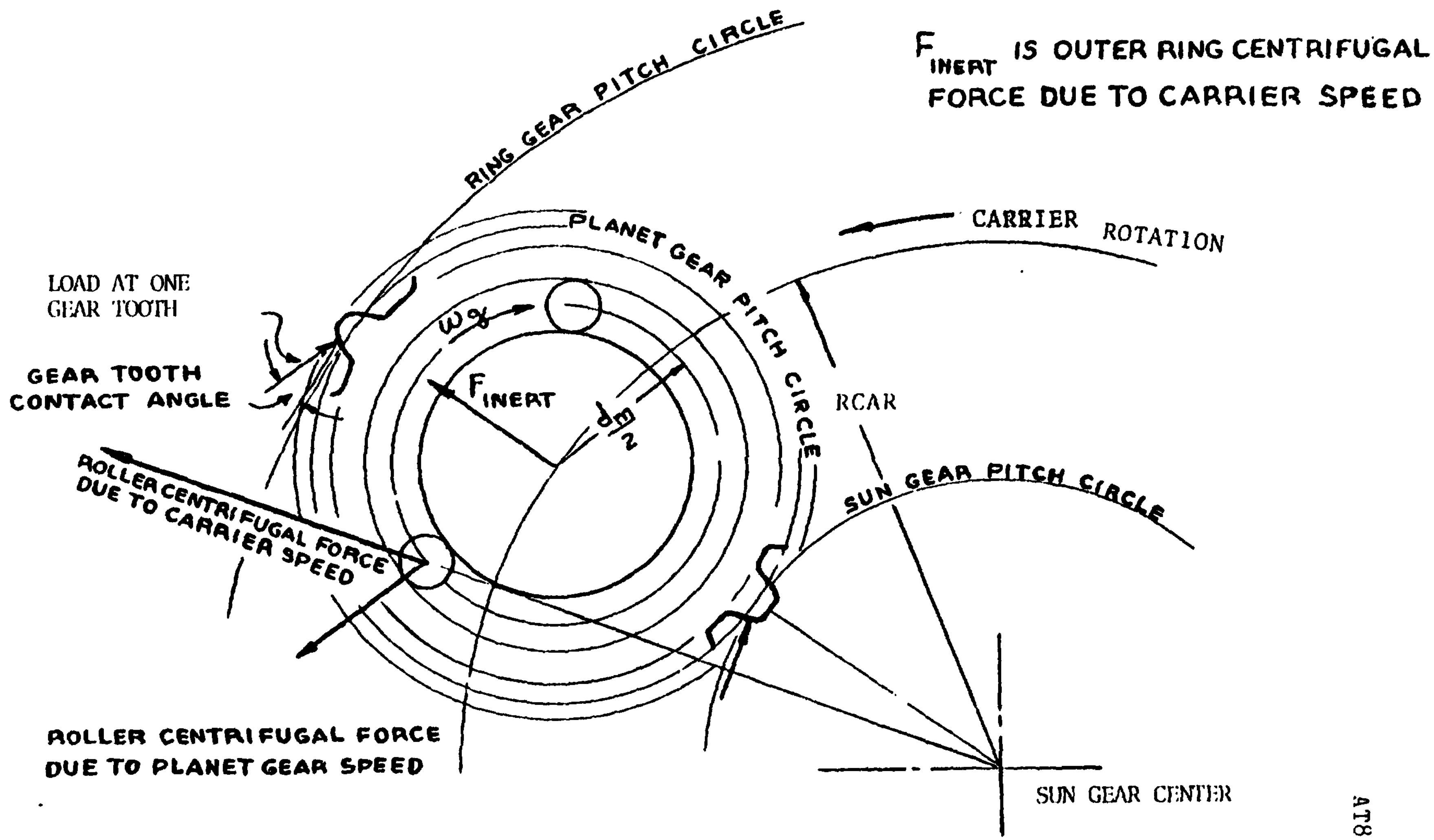

AT81D006

FIGURE 13: HIGH SPEED PLANET GEAR LOADING

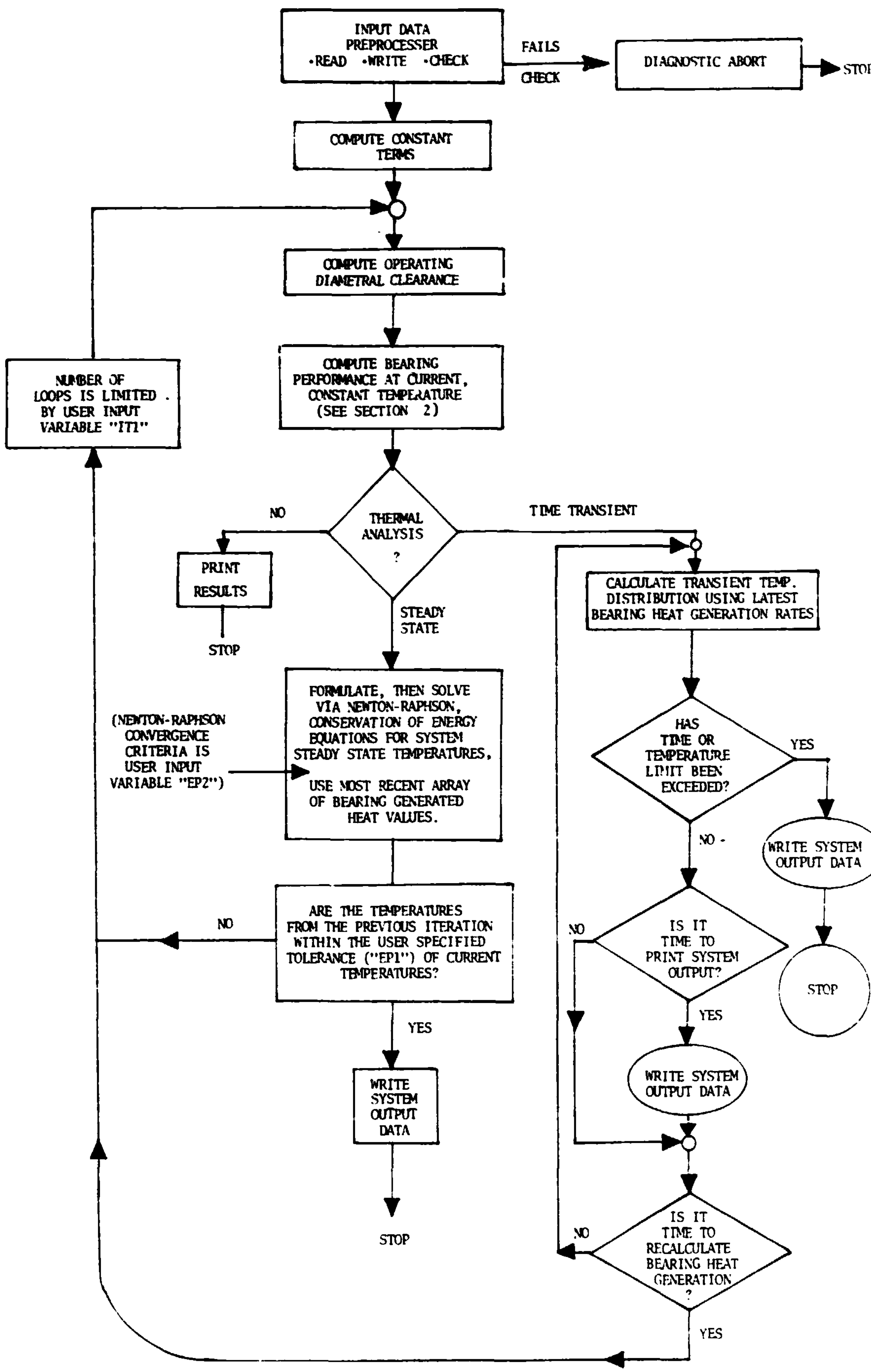

FIGURE 14: SIMPLIFIED FLOW CHART FOR SPHERBEAN

APPENDIX A

COORDINATE FRAME DEFINITIONS AND TRANSFORMATIONS

APPENDIX A:
COORDINATE FRAME DEFINITIONS AND TRANSFORMATIONS

Consider a double row spherical roller bearing, Figure A-1, and introduce a cartesian coordinate system $X_o - Y_o - Z_o$ such that the X_o axis is coincident with the bearing's outer ring longitudinal center line. Position the Y_o-Z_o plane along this centerline such that it contains the outer ring sphere origin, Figure A-2. The Y_o axis defines the angle $\phi = 0^o$ and the Z_o axis $\phi = 90^o$. Assume the X_o-Y_o-Z_o system to be fixed with respect to the outer ring, and the outer ring center of mass fixed in space.

Introduce a second system, X_I-Y_I-Z_I, initially coincident with the X_o-Y_o-Z_o system, but attached to the inner ring and free to move through space as the inner ring moves, Figure A-3.

A third coordinate system, X_R-Y_R-Z_R, is introduced at each roller location so that the X_R axis is along the roller centerline (rotation axis). The origin of the system is selected to lie on the line directed radially outward along the contact angle, Figures A-1 and A-4. The Z_R axis is tangent to the pitch circle. The X_R-Y_R-Z_R coordinate system is fixed in space in a radial position so that the clearance between the roller and raceway, at the point of closest approach, is equal to 1/4 the diametral clearance, Figure A-4.

Introduce a fourth coordinate system, $X_{\overline{R}}$-$Y_{\overline{R}}$-$Z_{\overline{R}}$, at each roller location. This system is initially coincident with the X_R-Y_R-Z_R system, but free to move through space as the roller moves.

RELATIONSHIPS BETWEEN COORDINATE SYSTEMS

It is frequently necessary to express the components of a vector in at least two coordinate frames. This is particularly so in the definition of bearing geometry, where initial specification is convenient in inertial coordinate frames. However, the bearing analysis frequently requires redefinition in frames which are in motion.

The linear orthogonal transformation operator, $[\Phi TS]$, describes the rotation portion of the transformation between "S" and "T" coordinate frames:

$$[\Phi TS] = \begin{bmatrix} \Phi_{11} & \Phi_{12} & \Phi_{13} \\ \Phi_{21} & \Phi_{22} & \Phi_{23} \\ \Phi_{31} & \Phi_{32} & \Phi_{33} \end{bmatrix} \qquad (1)$$

Six transformation operators will be defined, and from these all required transformations can be performed. They are:

1. Outer ring coordinate system (O) to the inner ring system (I).
2. Outer ring coordinate system to the i-th roller inertial system (R).
3. i-th roller inertial system to the i-th roller moving system ($\overline{R}$).

Transformations 4, 5, and 6 are the inverse of 1, 2, and 3.

Consider the transformation from the outer to inner ring frames:

$$[\Phi IO] = \begin{bmatrix} \cos\gamma_z \cos\gamma_y & \sin\gamma_z & -\cos\gamma_z \sin\gamma_y \\ -\sin\gamma_z \cos\gamma_y & \cos\gamma_z & \sin\gamma_z \sin\gamma_y \\ \sin\gamma_y & 0 & \cos\gamma_y \end{bmatrix} \qquad (2)$$

where: γ_z - rotation, or "misalignment angle" of outer ring about the Z_o axis[10].

γ_y - rotation of outer ring about the Y_o axis[10].

The inverse transformation, from the inner ring to outer ring frame, is given by the transpose of (2):

$$[\Phi OI] = \begin{bmatrix} \cos\gamma_z \cos\gamma_y & -\sin\gamma_z \cos\gamma_y & \sin\gamma_y \\ \sin\gamma_z & \cos\gamma_z & 0 \\ -\cos\gamma_z \sin\gamma_y & \sin\gamma_z \sin\gamma_y & \cos\gamma_y \end{bmatrix} \qquad (3)$$

Similarlv, we obtain the following for the remaining four transformation operations:

$$[\Phi RO] = \begin{bmatrix} \cos\alpha & -\sin\alpha \cos\phi_i & -\sin\alpha \sin\phi_i \\ \sin\alpha & \cos\alpha \cos\phi_i & \cos\alpha \sin\phi_i \\ 0 & -\sin\phi_i & \cos\phi_i \end{bmatrix} \qquad (4)$$

---

[10] In the current version of SPHERBEAN, $\gamma_y = \gamma_z = 0$.

F-4185C-1-R100

$$[\Phi OR] = \begin{bmatrix} \cos\alpha & \sin\alpha & 0 \\ -\sin\alpha\cos\phi_i & \cos\alpha\cos\phi_i & -\sin\phi_i \\ -\sin\alpha\sin\phi_i & \cos\alpha\sin\phi_i & \cos\phi_i \end{bmatrix} \quad (5)$$

$$[\Phi\bar{R}R] = \begin{bmatrix} \cos\gamma_t\cos\gamma_s & \sin\gamma_t & -\cos\gamma_t\sin\gamma_s \\ -\sin\gamma_t\cos\gamma_s & \cos\gamma_t & \sin\gamma_t\sin\gamma_s \\ \sin\gamma_s & 0 & \cos\gamma_s \end{bmatrix} \quad (6)$$

$$[\Phi R\bar{R}] = \begin{bmatrix} \cos\gamma_t\cos\gamma_s & -\sin\gamma_t\cos\gamma_s & \sin\gamma_s \\ \sin\gamma_t & \cos\gamma_t & 0 \\ -\cos\gamma_t\sin\gamma_s & \sin\gamma_t\sin\gamma_s & \cos\gamma_s \end{bmatrix} \quad (7)$$

In equations (4) through (7):

- α, the contact angle, is defined as positive for rollers in row 1 and negative for rollers in row 2, Figure A-1.
- γ_t is commonly referred to as the roller tilt angle, and represents the angular displacement of the roller about the $Z_{\bar{R}}$ axis.
- γ_s is commonly referred to as the roller skew angle, and represents the angular displacement of the roller about the Y_R axis.

F-4185C-1-R100

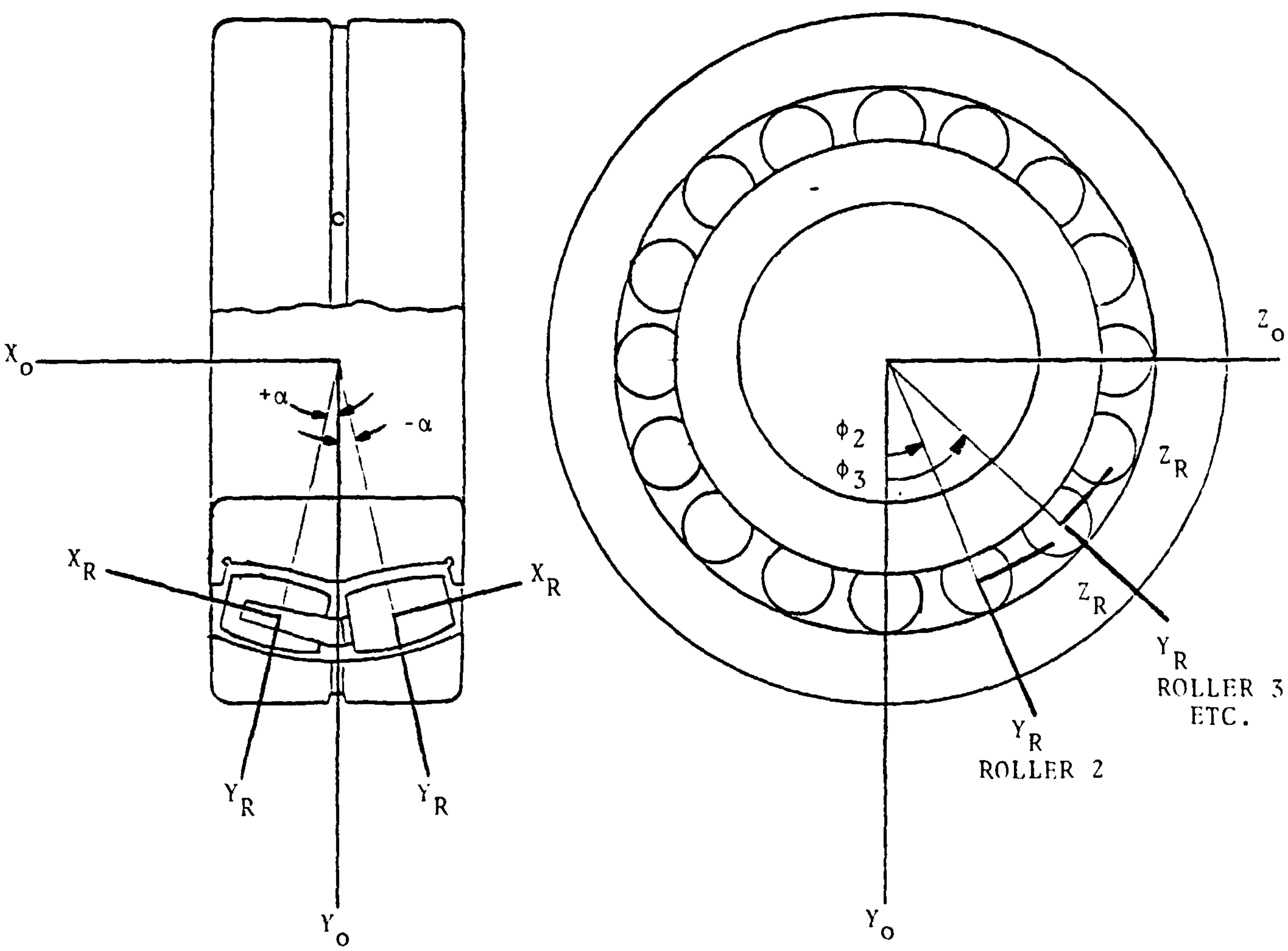

FIGURE A1: SPERICAL ROLLER BEARING COORDINATE FRAMES

AT81D006

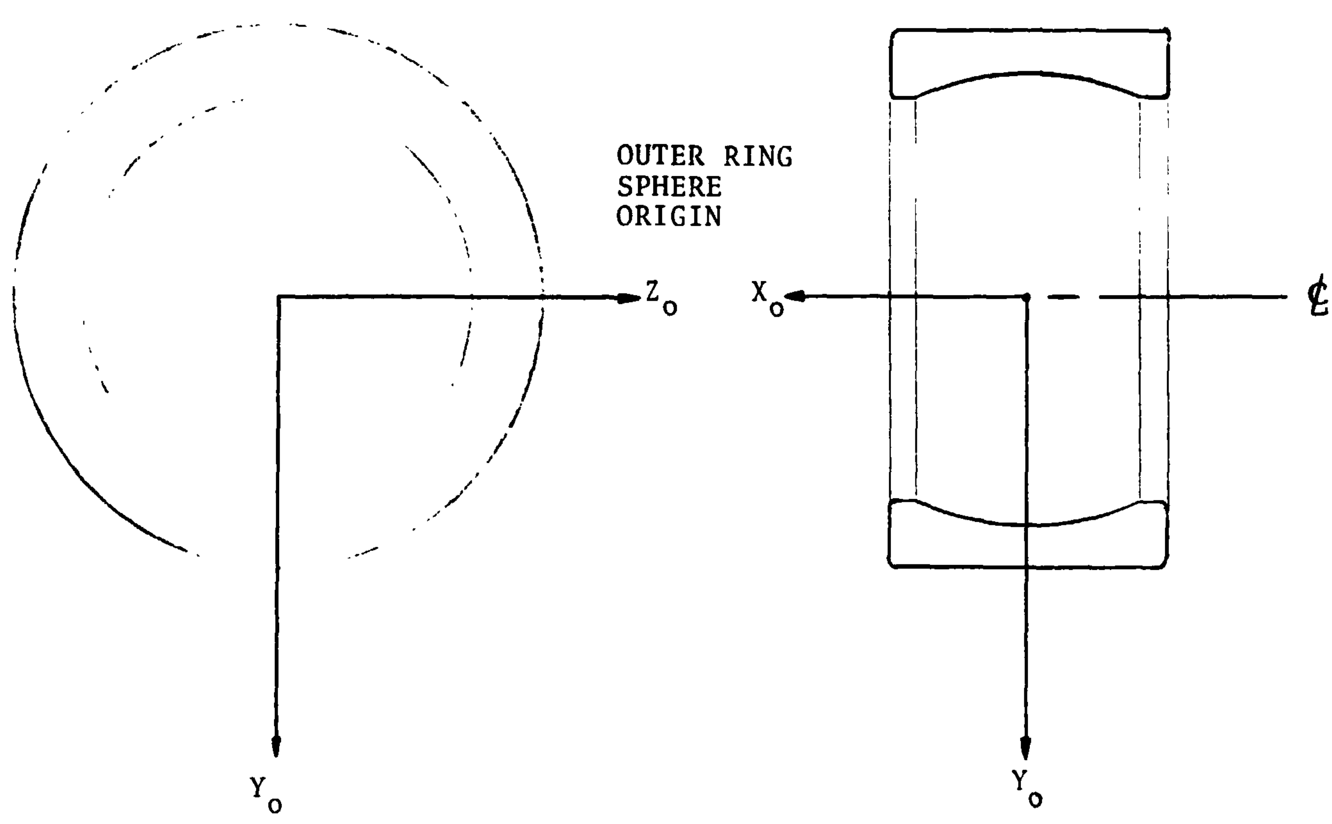

FIGURE A-2: OUTER RING COORDINATE SYSTEM

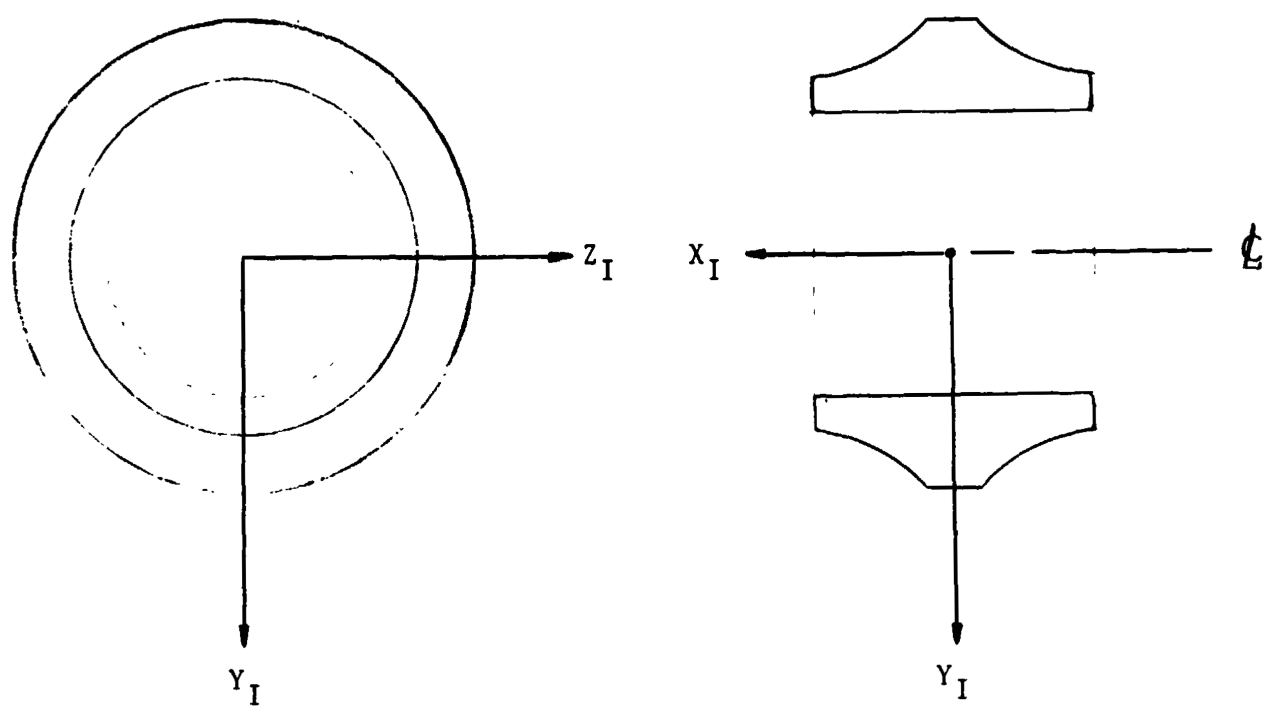

FIGURE A-3: INNER RING COORDINATE SYSTEM

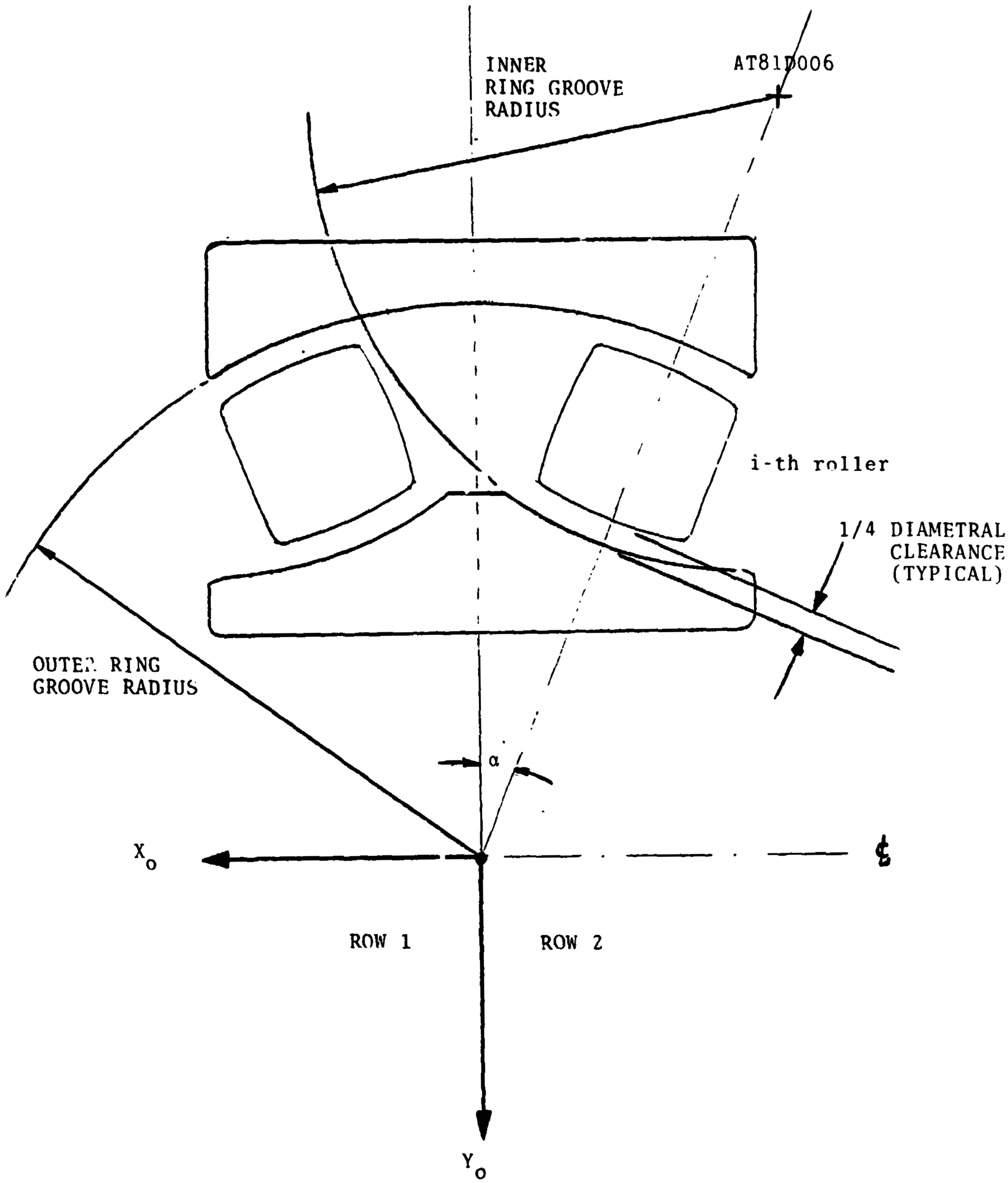

FIGURE A-4: BEARING GEOMETRY

APPENDIX B

FATIGUE LIFE COMPUTATION

INTRODUCTION

Within SPHERBEAN, roller bearing fatigue life is calculated using Lundberg-Palmgren [32,33] methods. The value computed is then modified by multiplicative factors which account for material and lubrication effects.

ROLLER BEARING RACEWAY LIFE

The load distribution across a line contact is represented by a number of slices. The L_{10} fatigue life of a given slice is:

$$L_{10mk} = \left(\frac{Q_{cmk}}{Q_{emk}} \right)^4 \qquad (1)$$

Here, Q_{cmk} is defi ed as the load for which a slice will have 90 percent assurance of surviving 1 million revolutions. Letting m refer to a raceway, k to a slice, where n is the index of the last slice, the explicit form of Q_{cmk} is given by [8]:

$$Q_{cmk} = \frac{49500\ \lambda\ \{D(1 \pm \gamma_m)\}^{1.074}\ \ell_m^{\ 0.778}\ (\gamma_m)^{0.222}}{\{N(1 \pm \gamma_m)\}^{0.25}} \qquad (2)$$

where:

N: is the number of rollers per row
λ: is the capacity reduction factor

$\lambda_k = .8$ when $k = 2, 3, \ldots, (n-1)$
$\lambda_k = .53$ when $k = 1$ or $k = n$

Note that the upper sign is used for the outer race, the lower sign for the inner race.

Q_{emk} is the equivalent load for the slice:

$$Q_{emk} = \frac{1}{n_r} \left(\sum_{j=1}^{n_r} Q_{mkj}^{\varepsilon} \right)^{1/\varepsilon} \qquad (3)$$

Q_{mkj} is the individual contact load on the k-th slice and $\varepsilon = 4.0$ or $\varepsilon = 4.5$, depending respectively upon whether the applied load rotates or is stationary with respect to the raceway in question.

L_{10} life of a raceway is given by

$$L_{10m} = a_2\ a_3\ a_4 \left[\sum_{k=1}^{n} (L_{10mk})^{-e} \right]^{-1/e} \qquad (4)$$

where e is the Weibull slope exponent, here taken to be 9/8, and

a_2 is a life improvement factor to account for improved materials (User input to program, see [35] factors "D" and "E.")

a_3 is a life factor to account for film thickness to surface roughness ratio (computed within SPHERBEAN [34]; factor "F" in [35]).

a_4 is a factor which accounts for materials having a modulus of elasticity other than that of basic steel (computed within SPHERBEAN).

BEARING LIFE

L_{10} life of a single row bearing, considering both raceways, is:

$$L_{10} = \{ \sum_{m=1}^{2} (L_{10m})^{-e} \}^{-1/e} \quad (5)$$

If the bearing contains two rows of rollers, each row can be treated as a separate bearing and the lives summed to yield the double row bearing life

$$L_{10} = \{ (L_{10_{ROW\ 1}})^{-e} + (L_{10_{ROW\ 2}})^{-e} \}^{-1/e} \quad (6)$$

APPENDIX C: THERMAL MODEL

TEMPERATURE CALCULATIONS

After each calculation of bearing generated heat rates, either steady state or time transient temperature analysis may be performed. The computations are terminated in the following manner:

1. The steady state case terminates when each system node temperature is within Δ °Centigrade of its previously predicted value. The value for Δ is specified by the user (typically 2°C).
2. The transient calculation terminates when the user specified transient time interval is reached or when one of the system temperature nodes exceeds 600°C (1112°F).

STEADY STATE TEMPERATURE MAP

The physical structure is considered to be divided into a number of elements represented by nodes. Heat fl to node i from surrounding nodes j, plus the heat generated at node i, must equal zero to satisfy the definition of steady state conditions.

After each calculation of bearing generated heat, which results from a solution of the bearing portion of the program, a set of system temperatures is determined which satisfy:

$$q_i = q_{oi} + q_{gi} = o \text{ for all nodes } i \qquad (1)$$

where q_{oi} is the heat flow from all neighboring nodes to node i

q_{gi} is the heat generated at node i. Values are calculated to represent heat created by bearing friction.

The resulting set of field equations is solved with a modified Newton-Raphson method which successfully terminates when

$$\sum_{i=1}^{n} \left[\frac{(EQ)_i^2}{n}\right]^{1/2} < \delta \qquad (2)$$

where,

n = number of field equations

EQ_i = residue of the i-th field equation

δ = .01

TRANSIENT TEMPERATURES

The net heat q_i transferred to the i-th node heats the element, i.e.:

$$\rho C_{p_i} \quad V_i \quad \frac{dt_i}{dT_i} = q_i \qquad (3)$$

where

ρ = density

C_p = specific heat

V = volume of the element

t = temperature

T = time

The temperatures, t_{oi}, at the time of initiation $T=T_s$ are assumed › be known, that is

$$t_{oi} = t_i \ (T_s) \qquad i = 1,2,\ldots,n \tag{4}$$

The problem of calculating the transient temperature distribution in a bearing configuration thus becomes a problem of solving a system of nonlinear differential equations of the first order with prescribed initial conditions. The equations are nonlinear since they contain radiation terms and free convection, which are nonlinear with temperature as will be shown later. The simplest and most economical way to arrive at a solution is to calculate the rate of temperature increase at the time $T = T_k$ from equation (3) and then compute the temperatures at time $T_k + \Delta T$ from

$$t_{k+1} = t_k + \frac{dt_k}{dT} \Delta T = t_k + \frac{q_k}{\rho C_p V} \cdot \Delta T \tag{5}$$

CALCULATION OF TRANSIENT TIME STEP

If the time step ΔT used is chosen too large, the temperatures will oscillate; if it is chosen too small, the calculation will be costly. It is therefore desirable to choose the largest possible time step that does not give an oscillating solution [36, 37] :

$$\frac{dt_{i,k+1}}{dt_{i,k}} \geqslant 0 \qquad i = 1, 2, \ldots, n \tag{6}$$

If this derivative were negative, the implication would be that the local temperature at node i has a negative effect on its future value. This would imply that the hotter a region is now, the colder it will be after an equal time interval. An oscillating solution would result.

Differentiating (5) for node i and combining with (6), the time step size condition is

$$\frac{dt_{i,k+1}}{dt_{i,k}} = 1 + \frac{\Delta T_i}{\rho_i C_{p_i} V_i} \quad \frac{dq_i}{dt_i} \geqslant 0 \qquad (7)$$

The derivative dq_i/dt_i is approximated using the forward difference operator

$$\frac{dq_i}{dt_i} = \frac{q_i\ (t_i + \Delta t_i) - q_i(t_i)}{\Delta t_i} \qquad (8)$$

The values ΔT_i which satisfy the equality in equation (7) are calculated. The array is searched, and a value of ΔT , rounded off to one significant digit smaller than the smallest of the ΔT_i obtained is used.

CALCULATION OF HEAT TRANSFER RATE

Heat transfer mechanisms which occur in a bearing application are:

- Conduction between inner ring and shaft and between outer ring and housing
- Convection between the surface of the housing and the surrounding air.

- Radiation between the shaft and the housing.
- Forced convection between the bearing and circulating oil.

All the above mentioned modes of heat transfer are considered in calculations of the heat balance at each given node.

GENERATED HEAT

A heat source may exist at node i. The quantity representing the source magnitude must be added to the net heat flowing from neighboring nodes.

When the heat source is other than a spherical roller bearing, it may be considered to produce known amounts of power, in which case constant numbers are entered as input to the program (see Example 1 in [11]).

CONDUCTION

The heat flow $q_{ci,j}$ which is transferred by conduction from node i to node j, is:

$$q_{ci,j} = \frac{\lambda A}{\ell} (t_i - t_j)$$

where λ = the thermal conductivity of the medium
ℓ = length between i and j

FREE CONVECTION

Free convection between a solid medium and air, the heat flow $q_{vi,j}$ transferred between nodes i and j can be calculated from the equation

$$q_{vi,j} = \alpha_v A \ |t_i - t_j|^d \ . \ \mathrm{SIGN}\ (t_i - t_j) \qquad (10)$$

where

α_v = the film coefficient of heat transfer by free convection

A = the surface area of thermal contact between the media

d = is an exponent, usually = 1.25, but any value can be specified as imput to the program

$$\mathrm{SIGN} = \begin{cases} 1 \text{ if } t_i > t_j \\ -1 \text{ if } t_i < t_j \end{cases}$$

The value of α_v can be calculated for various cases [36, 38].

FORCED CONVECTION

Heat flow $q_{wi,j}$ transferred by forced convection can be obtained from the following equation.

$$q_{wi,j} = \alpha_w A(t_i - t_j) \qquad (11)$$

where α_w is the film coefficient of heat transfer during forced convection. This value is dependent on the actual shape, the surface condition of the body, the difference in speed, as well as the properties of the liquid or gas [38].

In most cases, it is possible to calculate the coefficient of forced convection from a general relationship of the form,

$$N_u = aR_e^b P_r^c \qquad (12)$$

F-4185C-1-R100

where a, b, and c are constants obtained from handbooks, [39],

R_e and P_r are dimensionless numbers defined by

N_u = Nusselt number = $\alpha_w L/\lambda$
L = characteristic length
λ = conductivity of the fluid
R_e = Reynold's number = $UL\rho/\eta$
U = characteristic speed
ρ = density of the fluid
η = dynamic viscosity of the fluid
P_r = Prandtl's number = $\eta C_p/\lambda$
C_p = specific heat

SPHERBEAN can accept a specified constant value for the coefficient of convection, or, at the user's option, the coefficient can be calculated internally by the program. If the calculation option is exercised, input can be given in one of three ways:

Constant Viscosity

1. Values of the parameters in Equation (12) are given as input and a constant value of α_w is calculated by the program.

Temperature Dependent Viscosity

2. The coefficient α_w for turbulent flow and heating of petroleum oils is given by

$$\alpha_w = k_9 \cdot \{\eta(t)\}^{k_{10}}$$

where k_9 and k_{10} are given as input together with viscosity at two different temperatures.

F-4185C-1-R100

3. Values of the parameters in Equation (12) are given as input. Viscosity is given at two different temperatures.

RADIATION

If two flat, parallel surfaces of same surface area A, are placed close together, the heat transferred by radiation between nodes i and j representing those bodies, will be,

$$q_{Ri,j} = \varepsilon\sigma A\ [(t_i + 273)^4 - (t_j + 273)^4] \qquad (14)$$

here, ε is the surface emissivity, and σ is the Stefan-Boltzmann radiation constant.

Heat transfer by radiation under other conditions can also be calculated [36,38]. The following equation, for instance, applies between two concentric cylindrical surfaces:

$$q_{Ri,j} = \frac{\varepsilon\sigma A_i\,[(t_i + 273)^4 - (t_j + 273)^4]}{1 + (1-\varepsilon)\ (A_i/A_e)}$$

where A_i is the area of the inner cylindrical surface

A_e is the area of the outer cylindrical surface

FLUID FLOW

Between nodes established in fluids, heat is transferred by transport of the fluid itself and the heat it contains.

Figure C-1, on the following page, shows nodes i and j at the midpoints of consecutive segments established in a stream of flowing fluid.

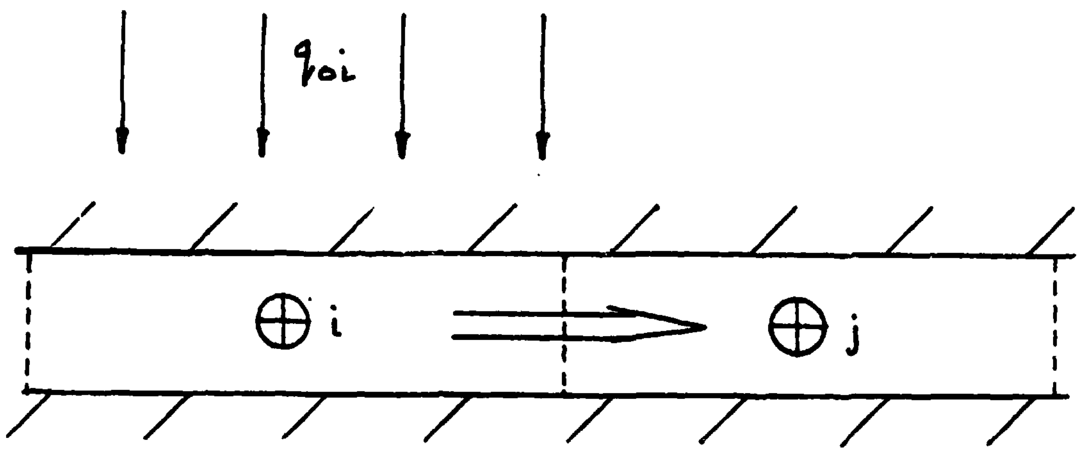

FIGURE C-1: FLUID HEAT NODES

The heat flow $q_{ui,j}$ through the boundary between nodes i and j can be calculated as the sum of the heat flow q_{fi} through the middle of the element i, and half the heat flow q_{oi} transferred to node i by other means, eg., convection.

The heat carried by mass flow is,

$$q_{fi} = \rho_i \, C_{p_i} \, V_i \, t_i = K_i t_i \tag{16}$$

where V_i = the volume flow rate through node i.

The heat input to node i is the sum of the heat generated at node i (if any) and the sum over all other nodes of the heat transferred to node i by conduction, radiation, free and forced convection.

$$q_{oi} = q_{G,i} + \sum_j (q_{ci,j} + q_{vi,j} + q_{wi,j} + q_{Ri,j}) \tag{17}$$

The heat flow between the nodes of Figure C-1 is, then,

$$q_{ui,j} = q_{fi} + q_{oi}/2 \tag{18}$$

If the flow is dividing between node i and j, as in Figure C-2, then the heat flow is calculated from

$$q_{ui,j} = K_{ij} \, (q_{fi} + q_{oi}/2) \tag{19}$$

where k_{ij} = the proportion of the flow at i going to node j,

$$0 \leqslant K_{ij} \leqslant 1.$$

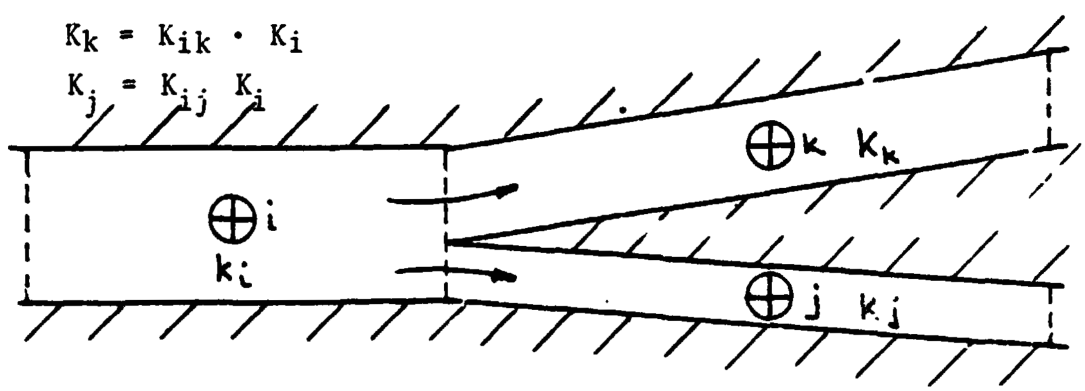

FIGURE C-2: DIVIDED FLUID FLOW FROM NODE i

TOTAL HEAT TRANSFERRED

The net heat flow rate to node i can be expressed as,

$$q_i = q_{G,i} + \sum_j (q_{ci,j} + q_{ui,j} + q_{vi,j} + q_{wi,j} + q_{Ri,j}) \tag{20}$$

The summation should include all nodes j, which interact with i. Unknown temperatures as well as those specified as known should be included.

F-4185C-1-R100

CONDUCTION THROUGH A BEARING

The conduction between two nodes is governed by the thermal conductivity parameter λ. The value of λ is specified at input.

An exception occurs when one of the nodes represents a bearing ring and the other a set of rolling elements. Here, the conduction is calculated separately by the program using the principles described below.

THERMAL RESISTANCE

It is assumed that the rolling speeds of the rolling elements are so high that the bulk temperature of the rolling elements is the same at both the inner and outer races, except in a volume close to the surface. The resistance to heat flow can then be calculated as the sum of the resistance across the surface and the resistance of the material close to the surface.

The resistance Ω is defined implicitly by

$$\Delta t = \Omega \cdot q \qquad (21)$$

where Δt is the temperature difference
and q is the heat flow

The resistance due to conduction through the EHD film is calculated as

$$\Omega_1 = (h/\lambda) \cdot A \qquad (22)$$

F-4185C-1-R100

where h is taken to be the calculated plateau film thickness

A is the Hertzian contact area at the specific rolling element-ring contact under consideration.

λ is the conductivity of the oil.

The geometry is shown in Figure C-3 (a). Asperity conduction is not considered.

So far, a constant temperature difference between the surfaces has been assumed. But during the time period of contact, the difference will dec e because of the finite thermal diffusivity of the material near the surface, Figure C-3(b).

To points at a distance from the surface, this phenomenon will have the same effect as an additional resistance Ω_2 acting in series with Ω_1.

This resistance was estimated [40] as,

$$\Omega_2 = \frac{1}{\lambda \ell_{re,i}} \left(\frac{\pi\psi}{2b_i V}\right)^{1/2}$$

where ℓ_{re} = contact length, or in the case of an elliptical contact area, 0.8 times the major axis.

λ = heat conductivity

ψ = thermal diffusivity = $\lambda/(\rho . C_p)$

ρ = density

C_p = specific heat

b = half the contact width

V = rolling speed

The resultant resistance is

$$\Omega_{res} = \Omega_1 + \Omega_2 \tag{24}$$

There is one such resistance at each rolling element. Thev all act in parallel. The resultant resistance, Ω_{res}, is thus obtained from

$$\frac{1}{\Omega_{res}} = \sum_{i=1}^{n} \frac{1}{\Omega_{res,i}} \tag{25}$$

AT81D006

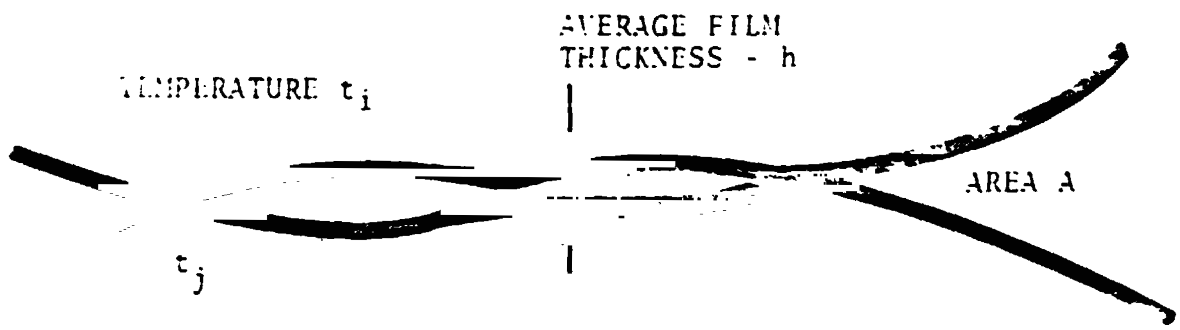

(a) Schematic Concentrated Contact

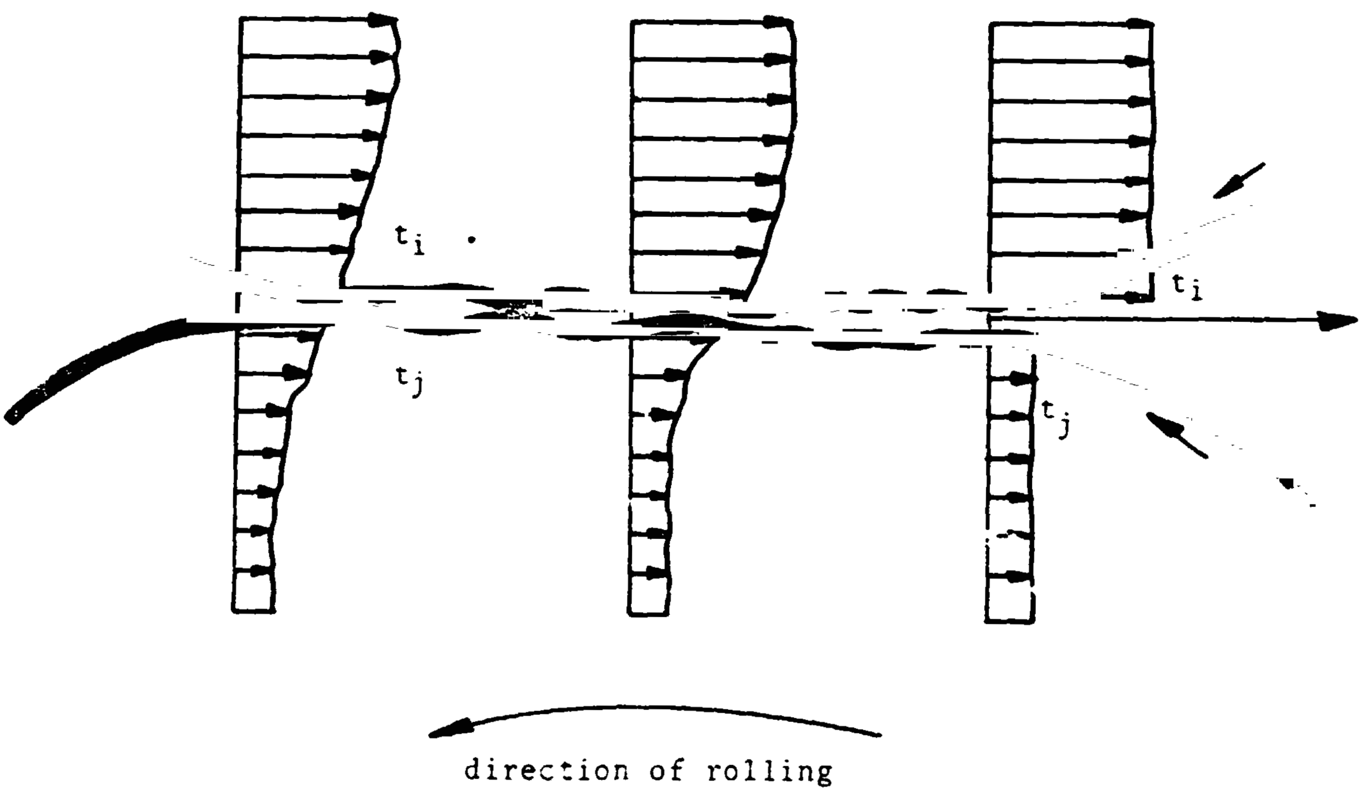

(b) Temperature Distribution at Rolling, Concentrated Contact Surfaces

FIGURE C-3: CONTACT GEOMETRY AND TEMPERATURES